Mathematical Simulation of A Dipole Delivery System for In-situ Remediation

by

Chao Huo

A thesis

presented to the University of Waterloo

in fulfillment of the

thesis requirement for the degree of

Master of Applied Science

in

Civil Engineering

Waterloo, Ontario, Canada, 2010

Author's Declaration

I hereby declare that I am the sole author of this thesis. This is a true copy of the thesis, including any required final revisions, as accepted by my examiners.

I understand that my thesis may be made electronically available to the public.

Abstract

In-situ remediation using reactive zones is a promising groundwater contaminant treatment technology that involves the injection of a reagent(s) into the subsurface to destruct harmful target chemicals. For efficient and effective treatment the reagent has to be delivered into a specific contaminated zone for the desired chemical reaction(s) to occur. The most commonly used delivery method is a conventional well where the distribution of injected reagent is mainly controlled by the surrounding hydraulic conductivity field. In this case, the reagent is easily delivered into the higher hydraulic conductivity zones but the lower hydraulic conductivity zones are missed. The goal of this research effort is to investigate a novel delivery method involving a single well vertical recirculation system or a dipole well. The configuration of this single dipole well is that injection and extraction occurs from two chambers separated by an impermeable central packer. Thus, this dipole well system can induce predominantly vertical flow across bedding plane features and it is therefore hypothesised that this delivery system can overcome physical heterogeneities creating a more uniform reactive zone. The objective of this research was to demonstrate that the dipole well is a useful delivery tool compared to the commonly used single injection well.

Mathematical simulations were used to investigate the delivery performance of a dipole well using steady-state and transient approaches. A simple analytical model was used to determine the steady-state dipole flow field and observe the impact of system parameters on reagent delivery behaviour. The size of coverage area (the area swept by the injected reagent) was used as the performance metric to assess the impact of each system parameter on the dipole

well performance. Numerical simulations were used to extend this investigation to homogeneous and heterogeneous (structured or randomly correlated hydraulic conductivity) aquifers under pulsed operation to identify those situations where the dipole delivery system is more efficient or effective. Both forward and backward particle path lines were used to identify reagent coverage areas around the injection well and down gradient. The impact of each system parameters on the dipole well performance was studied.

The shoulder length and the injection cost are characteristic parameters that affect dipole delivery performance. A relationship between the down gradient coverage area vs. characteristic system parameters was developed and can be used to predict the dipole well performance in homogenous aquifers. The impact of the hydraulic conductivity distribution on dipole well performance is consistent with either a structured hydraulic conductivity field or randomly correlated hydraulic conductivity fields. Regions of lower hydraulic conductivity can be swept by the dipole well and the dipole well outperforms a single injection well, which is analyzed as a base case in terms of the shape of down gradient coverage area. However, the advantage of dipole well over a single well delivery is small if the degree of heterogeneity is large or the horizontal extent of the bedding plane is small.

Acknowledgements

First and most important, I would like to thank my supervisor Neil Thomson for accepting me to this program, and giving me tremendous help, encouragement, and guidance for my research. It took him lots of time to help me with my thesis and his patience really impressed me. I would also like to express my gratitude to my co-supervisor James Craig for giving me so many valuable instructions about solving the problems in the process of research.

Many other graduate students at the University of Waterloo, who shared their research experience and expertise with me, deserve special acknowledgement: Stefano Normani, Lucy Liu and Yong Yin. At the same time, I enjoy the time working with my officemates. They are awesome.

Last but not least, I would sincerely thank my family and friends, who give me support over the last three years.

Table of Contents

Appendices

List of Figures

List of Tables

Chapter One Introduction

Groundwater contamination sources are varied and include current and past agricultural and industrial activities (Patrick et al., 1987). In situations that involve point-sources, the contaminants are typically distributed between "source zones" (e.g., buried tanks, chemical spills, landfills, and coal tar deposits) and "plumes" (dissolved or vapor). When toxic substances are present, the resulting subsurface contamination may exceed regulatory standards prompting the need for clean-up of both the source zone and plume (Rail, 2000). In general, remediation technologies can be categorized as complete source removal, source and/or plume containment, and mass reduction methods. Some shallow contaminant sources can be located and either completely or partially removed. For deeper sources in-situ source zone treatment will be required particularly if non-aqueous phase liquids (NAPLs) are present or if contaminants have sorbed to the sediments. Dissolved phase plumes are mobile and therefore develop down gradient of the source zone. Depending on the strength of the source and natural attenuation mechanisms, the dissolved plume may be of significant spatial extent (Nyer et al., 2001) and be the risk driver for site clean-up (USGS, 1996).

In the 1980's and early 1990's, groundwater pump and treat (P&T) (Boulding, 1996) was used almost universally as a clean-up technology to remove mass from the source zone or to contain the dissolved plume. While P&T has been shown to work well for plume containment, it is very ineffective for mass removal from source zones (Mackay and Cherry, 1989; USEPA, 2003). Other technologies such as soil vapor extraction and in-situ air sparging are more cost effective than P&T in most cases but suffer from the same requirement as P&T: all of these technologies require an above ground treatment system to handle the extracted contaminant

mass. An alternative to these mass extraction technologies are those that provide in-situ mass destruction. The objective of in-situ mass destructive technology is to create reaction conditions in the subsurface so that when the contaminants are either contacted or intercepted they are immobilized or degraded into non-toxic end products. For dissolved plume treatment there are two general methods to create the required reactive zone: (1) direct contaminated groundwater through an engineered reactive system such as a funnel-and-gate (F&G) system (Starr, 1994), permeable reactive barriers (PRB) (USEPA 1998), or groundwater recirculation well (Cunningham, 2004), or (2) to allow the undisturbed subsurface to distribute the injected reagents to support the necessary reactive conditions. To be less invasive and avoid the infrastructure cost associated with technologies such as F&G and PRB, the second method to create a subsurface reactive zone is preferred and hence is the focus of this research effort. Both microbial (e.g., aerobic biostimulation, enhanced reductive dechlorination) and chemical reactions (e.g., oxidation, reduction, precipitation) can be used to treat a wide range of organic, inorganic and metallic contaminants (Sturman, 1995; Martin, 2004). For efficient and effective treatment to occur the selected reagents must be delivered into the in-situ reactive zone and the resulting biogeochemistry must be close to optimal for the desired reaction(s) to occur. Aside from reagent selection, uniform delivery of the reagent to the subsurface reactive zone is a necessary requirement for treatment (Seol, 2003).

The injection and distribution of treatment reagents is a challenging task due in part to the uncertain subsurface geological and contaminant characteristics, and the role of heterogeneity in soil properties that exists at all spatial scales. Hydraulic conductivity is perhaps the most critical property since this will control the ease at which a reagent can be delivered.

Groundwater flow characteristics can affect reactive zones by controlling the rate at which the reagent will spread and mix with the groundwater. Also important is the role that stagnant groundwater zones play in treatment. At the pore-scale, flow regimes can be represented by advective and static pore water zones. An injected reagent will flow through the advective zones but be limited by diffusion into the static zones (Bagagaoglu, 2002). This dual-porosity pore scale phenomena within a mildly heterogeneous aquifer can lead to incomplete reagent coverage and affect treatment performance.

The most commonly used method to delivery reagents into the reactive zone is injection wells or direct push well points. Other methods include gravity driven flooding using infiltration trenches/galleries, horizontal wells for shallow plumes beneath buildings, and a recirculation well system with extraction and injection wells (Boulding, 1996; Sawyer, 1998). For plume treatment in high-permeability aquifers single wells can be placed along a transect transverse to the plume flow direction and reagents injected in pulse-mode so that overlapping reactive zones are developed (Figure 1.1(a)). In aquifers where transverse dispersion is minimal, the primary mechanism for mixing with the groundwater plume is longitudinal dispersion (Sudicky，1986). A variation of the single well method is to establish a closed recirculation system in which one well is used as an injection well and the other as an extraction well (Figure 1.1(b)). This horizontal dipole system is operated until the reagent has reached the extraction well at sufficient concentration. The injected reagents then migrate down gradient under the natural gradient conditions before the next injection/extraction episode is started.

The ability of these natural gradient systems to mix the injected reagent solution with the dissolved contaminant plume depends on achieving sufficient lateral coverage at the time of

injection and the strength of the longitudinal mixing mechanisms. The performance of a single well to create a uniform spatial zone of coverage depends largerly on the hydraulic conductivity of the surrounding formation, and to a lesser degree on well performance issues and the nature of the disturbed or skin zone formed during well installation (Seol et al, 2003; Peursema, 1999). For example if a well screen was completed in a sedimentary deposit where interbedded sands and silts are present then the location and spatial extent of the high permeable sands will dominant the migration of the injected reagent solution. A potential method to overcome the role that layered sediments play on the spatial distribution of the injected reagent solution is to force the injected solution to migrate across the lower permeable layers using, for example, a single well vertical dipole system (Figure 1.1(c)).

The single well vertical dipole system was originally introduced by Kabala (1993) as a tool for estimating in-situ hydraulic conductivity and storativity called the dipole flow test (DFT). The DFT uses isolated extraction and injection chambers in a single well to create a predominantly steady-state vertical flow field. Pressure transducers are used to monitor hydraulic head changes in each chamber. These pressure data in conjunction with an interpretation model are used to estimate the radial hydraulic conductivity (K_r). Numerous DFTs have been conducted in various diameter wells with different dipole configurations and flow rates and estimated hydraulic conductivity along the horizontal plane K_r profiles generated from DFTs have shown similar trends and values to K estimates obtained through grain size analysis, permeameters, sieve analyses, flowmeters, and pumping tests (Zlotnik et al., 1998; Zlotnik et al., 2001; Zlotnik et al., 2003).

Sutton et al. (2000) extended the DFT by adding a suite of conservative tracers; thus creating a dipole flow and tracer test (DFTT). The DFTT works in a similar fashion to the DFT except when a steady-state flow field has been established, a suite of conservative tracers are released into the injection chamber and the tracer concentration is monitored in the extraction chamber. Sutton et al. (2000) suggested that a combination of the chamber pressure changes and key properties of the tracer breakthrough curve (BTC) could be used to estimate the K_r and the longitudinal dispersivity (α_L) along the DFT flowpaths. Recently, the dipole flow and reactive tracer test (DFRTT) was proposed as in-situ aquifer parameter estimation method (Thomson et al., 2005) and has a similar setup to the DFT except that in addition to conservative tracers a suite of reactive tracers (e.g., sorbing, degrading, biodegrading, etc.) are injected either as a spike or for an extended period of time. The concentrations of the tracers and their breakdown products are monitored in the extraction chamber to produce a number of tracer BTCs. These BTCs can be interpreted using simulation models (Reiha, 2006) in conjunction with optimization tools to estimate key aquifer parameters. Roos (2009) constructed a dipole probe prototype and conducted more than 50 field tests in the unconfined sand aquifer at CFB Borden near Alliston, ON. The results of this work show that a connected dipole flow field can be established within a relatively homogenous aquifer.

The basic physical dipole configuration ((Figure 1.1(c)) is adjustable so that by changing the parameters of the dipole tool (upper chamber length $2\Delta_{upper}$, lower chamber length $2\Delta_{lower}$ and central packer length D) the zone of influence can be modified. This allows the remediation engineer to configure the dipole tool to suit the observed K_r profile estimated from a DFT. We hypothesis that in certain situations the dipole system can be used as an efficient and effective

reagent delivery tool for both plume and source zone remediation. The objective of this research is to use simulation tools to determine a suite of scenarios where the use of the single well dipole system for reagent delivery would create an in-situ reactive zone that is more efficient and effective compared to a conventional single well.

1.1 Thesis Objectives

The goal of this research is to determine whether a dipole well can be a useful delivery method in terms of creating a reactive zone of a larger subsurface volume compared to that of the single well. The following objectives were defined:

- Use a simple analytical model to determine the steady-state dipole flow field and observe the impact of system parameters on the reagent delivery behaviour;
- Identify when the dipole well can outperform the delivery capabilities of a single well in a homogeneous aquifer under pulsed operation; and
- Extend the performance comparison to heterogeneous aquifers and identify those situations where the dipole delivery system is more efficient or effective.

1.2 Thesis Scope

Analytical and numerical models are used to simulate the behavior of a dipole or single well in homogeneous and heterogeneous aquifers. Chapter 2 focuses on the use of an analytical model to provide insight into the flow behavior of the dipole system under steady-state conditions in a homogeneous aquifer. Chapter 3 contains numerical modeling efforts which address the delivery capabilities of the dipole system under transient conditions in

homogeneous and heterogeneous aquifers. Finally, Chapter 4 presents the relevant conclusions and recommendations from this research.

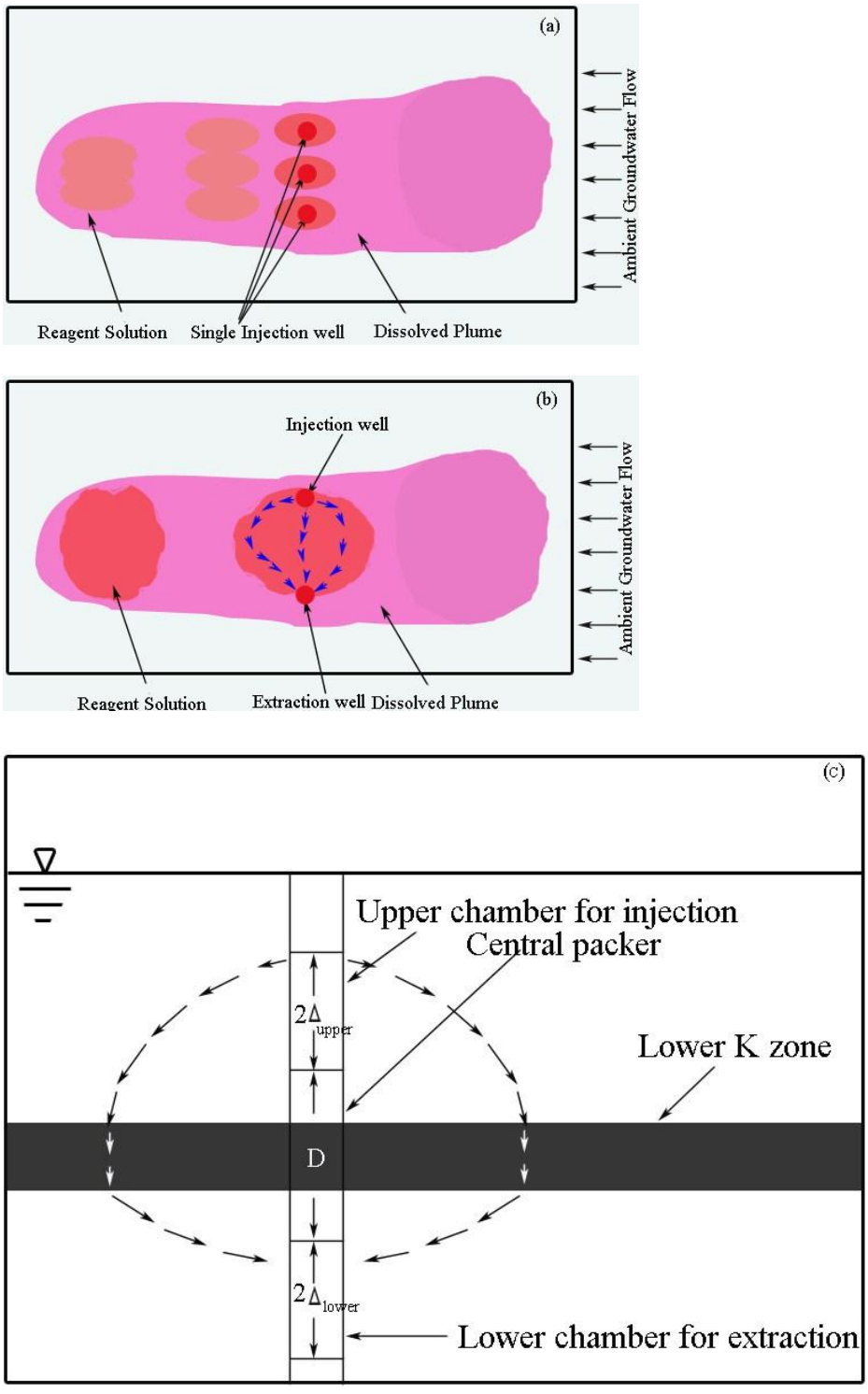

Figure 1.1. Schematic of the aquifer system showing: (a) the plan view of plume treatment using a single well pulsed injection system; (b) the plan view of plume treatment using a horizontal dipole well pulsed injection system; and (c) the profile view of a vertical dipole well reagent delivery system straddling a lower hydraulic conductivity layer.

Chapter Two Steady-State Dipole Behavior

To assess the ability of a dipole system to deliver reagent solution into a contaminated zone, an investigation into steady-state dipole behavior in a homogeneous aquifer was performed. Particle tracking was used to delineate the coverage area (Figure 2.1) which is determined by the dipole configuration (chamber length, packer length, and injection rate) and ambient aquifer conditions. A sensitivity analysis was conducted to study how these parameters can influence the dipole performance, using coverage area as a surrogate for performance. For comparison purposes, the performance of a single injection well is also investigated.

2.1 Steady-State Flow Model: DIPOLE3D

The simulations performed in this chapter use the DIPOLE3D software package (Craig, 2009) which can simulate the three-dimensional flow field created by either a dipole or a single well in a homogeneous aquifer under steady-state conditions. The dipole well is represented by an infinitely thin line sink (extraction chamber) and a line source (injection chamber), which are defined as a collection of point sinks/sources. The single well is simulated by a line source. As shown in Figure 2.2, the length of line sink/line source is equal to the length of the well chambers (2Δ) and the separation distance between the line source and line sink is equal to the central packer length (D). The final solution for the flow field in the vicinity of the dipole system is the summation of the influence of a line source, a line sink, and the influence of regional flow. For a single well, the final solution is the summation of the influence of only a line source and ambient flow. The flow field is obtained using the analytic solutions presented by Steward and Jin (2003). Once the flow field is calculated, particle tracking is performed

using the fourth-order Runge Kutta method described by Craig (2004). Complete information about DIPOLE3D refers to Craig (2009).

2.1.1 DIPOLE3D Governing Equations

Steady-state groundwater flow in a homogeneous aquifer is governed by the Laplace equation in terms of a discharge potential:

$$\frac{\partial^2 \phi}{\partial x^2} + \frac{\partial^2 \phi}{\partial y^2} + \frac{\partial^2 \phi}{\partial z^2} = 0, \tag{2.1}$$

with

$$\phi = Kh \tag{2.2}$$

where ϕ is the discharge potential [L^2/T], K is the hydraulic conductivity [L/T], and h is the hydraulic head [L]. Eq. (2.1) is in a Cartesian coordinate system with the origin located at the center of the packer (Figure 2.2).

2.1.2 DIPOLE3D Boundary Conditions and Constraints

The DIPOLE3D model calculates the flow field by enforcing boundary conditions along the well and at an infinite distance from the well. Along the well, the hydraulic head is assumed to be uniform, and the net injection/extraction rate of the well is fixed at the specified flow rate, Q. At the infinite distance from the well, the dipole influence diminishes to zero and the hydraulic head is only influenced by the ambient flow. Therefore, the hydraulic head gradient at infinity is the ratio between ambient Darcy flux and hydraulic conductivity q_0/K.

Note that the flow rate, Q, and ambient Darcy flux, q_0, are determined by hydraulic potential. For detailed information please refer to Steward and Jin (2003). The version of DIPOLE3D

used here does not account for the presence of the well casing and hence allows vertical flow towards/away from the ends of the dipole chambers. This results in a slightly different shape on the outer edges of the flow field and shorter travel times than might be expected in a real dipole system. Moreover, the DIPOLE3D model neglects the skin effect which describes the changes in hydraulic conductivity near the well borehole as a result of the installation process (Peursema, 1999). For the complete description of DIPOLE3D, please refer to Craig (2009).

2.1.3 DIPOLE3D Solution Method

The combined solution of the governing equation as in Eq. (2.1) subject to the boundary conditions simplifies when expressed in a local coordinate system. For each line segment, the mathematical representation of the potential in the local coordinate system is (Muskat, 1937):

$$\Phi_{\text{sink}} = -\frac{1}{4\pi}\int_{-L}^{L} \frac{\sigma_0 + \sigma_1\left(\frac{\hat{x}}{L}\right)}{[(x-\hat{x})^2 + y^2 + z^2]^{1/2}}\, d\tilde{x} \tag{2.3}$$

$$\Phi_{\text{src}} = \frac{1}{4\pi}\int_{-L}^{L} \frac{\sigma_0 + \sigma_1\left(\frac{\hat{x}}{L}\right)}{[(x-\hat{x})^2 + y^2 + z^2]^{1/2}}\, d\tilde{x} \tag{2.4}$$

$$\Phi_{f} = q_0 z \tag{2.5}$$

Where $\tilde{x}$ is the local coordinate along x-axis, Φ_{sink} is the potential due to the line sink segment [L^2/T], Φ_{src} is the potential due to the line source segment [L^2/T], Φ_f is the potential due to ambient flow [L^2/T], σ_0, σ_1 are the strength coefficients of the sink or source [L^2/T], $\hat{x}$ is the local x coordinate, which varies from zero at the center of this line sink to L at the end [L], L is the half-length of line segment [L], and q_0 is the ambient Darcy flux [L/T]. Note that the strength of each line sink or source segment is linear; the extraction or injection rate per unit length varies linearly from $(\sigma_0 - \sigma_1)$ at x = -L to $(\sigma_0 + \sigma_1)$ at x = L.

Eq. (2.3) and Eq. (2.4) are opposite in sign to represent inflow and outflow. Because the flow along a dipole chamber will not be linear, the solution is obtained by representing the wells using multiple line sinks/sources. For each line segment, the strength coefficients are unknown and have to be solved by applying the boundary conditions and constraints:

$$\mathrm{h(i)} = \mathrm{h(C)} \ \ (i = 1, \dots, \mathrm{N}) \tag{2.6}$$

$$\sum_{\mathrm{k}=1}^{\mathrm{n}} \mathrm{L_k}\sigma_{0\mathrm{k}} = \mathrm{Q} \tag{2.7}$$

where N is the number of collocation points; *n* is the number of line segments along the well, $\mathrm{h(C)}$ is the hydraulic head at each specified point C at each line segment [L/T], $\mathrm{h(i)}$ is the hydraulic head of the collocation points [L/T], $\mathrm{L_k}$ is the half length of *kth* line segment, and $\sigma_{0\mathrm{k}}$ is the coefficient σ_0 associated with the *kth* line segment.

The boundary condition (Eq. 2.6) is imposed by setting the hydraulic head at a set of N collocation points along the surface equal to the hydraulic head at a specified point along the well face boundary (Strack, 1989). Though this condition specifies that the hydraulic head is uniform along the cylindrical face of the chambers, the value of this hydraulic head is not known a priori but is obtained as a part of the solution.

The constraint Eq. (2.7) imposed is that the summation of flow rate for each line segment should be equal to the total flow rate. The boundary condition and the constraint are given by

$$\mathrm{h} = \mathrm{H} \ @ \ \ \mathrm{r} = \mathrm{r_w}, \mathrm{D} \leq \mathrm{x} \leq \mathrm{D} + 2\Delta \tag{2.8}$$

$$\sum_{\mathrm{i}=1}^{\mathrm{n}} \mathrm{Q_i} = \mathrm{Q} \tag{2.9}$$

where H is a constant [L], n is the total number of the segments, r_w is the radius of the chamber/well[L], D is the central packer length [L], Δ is the half chamber length [L], and Q_i is the pumping rate at ith line segment [L^3/T]. For a single injection well, D = 0. The application of the boundary conditions leads to a single system of linear equations to determine the strength coefficients σ_{0k} and σ_{1k} associated with all line segments. Eq. (2.6) can be decomposed into an unknown portion associated with strengths for the chamber/well ($\emptyset/K$ for the head of all line segments along the chamber/well) and a known portion associated with ambient flow (for a reference point). For each line segment with N collocation points, we have:

$$h|_{well}(i) - h|_{well}(C) = h|_{Rflow}(C) - h|_{Rflow}(i) \quad (i = 1, \dots, N) \qquad (2.10)$$

The combination of Eq. (2.10) for (i = 1,…,n) and Eq. (2.9) (i = n + 1) leads to a system of linear algebraic equations for the n + 1 unknowns:

$$\sum_{j=1}^{m} a_{ij} x_j = b_i \quad (i = 1, \dots, n+1) \qquad (2.11)$$

where x_j are the m = 2n priori unknown strength coefficients (each line segment has two strength coefficients σ_0, σ_1), and a_{ij} and b_i contain constants obtained from equations $i = 1$ to $i = n$ by evaluating the potential functions associated with Eq. (2.10) and for Eq. (n + 1) using Eq. (2.9). For a description of the solution of the system of equations refer to Steward and Jin (2003).

Once the coefficients are calculated, the final dipole flow solution (in terms of potential) can be obtained by transforming the solutions of the Eq.(2.3) – Eq.(2.5) from the local line segment coordinate system to the global Cartesian coordinate system and then summing each

line segment solution together with the solution for ambient groundwater flow (Appendix A). Flow rates and velocities (for particle tracking) may be obtained analytically from the gradients of the final discharge potential function. The detailed information of solving the governing equation can refer to Steward and Jin (2003).

2.1.4 Parameterization

The default geological properties for this investigation are consistent with those used by Roos (2009) and Reiha (2006). The homogeneous aquifer is assumed isotropic with a hydraulic conductivity (K) of 0.864 m/d and porosity of 0.3. For the base case, a steady injection rate (Q) of 2.0 m^3/d is used.

For the performance comparison between a fully-screened single well and the dipole system we have assumed a conventional well screen length of 1.5 m (5 ft) and diameter of 10 cm (4 inches). For the single well simulations the full 1.5 m length is used, while for the dipole simulations we consider various configurations that would work within a 1.5 m long well screen. Therefore, the maximum dipole length including two chambers and a central packer is:

$$4\Delta + D \leq 1.5 \text{ m} \qquad (2.12)$$

For the base case, the chamber length (2Δ) is set to 0.3 m and the central packer length is set to 0.9 m. For the sensitivity analysis, the chamber length, the central packer length, the flow rate, and the ambient gradient were varied (Table 2.1).

2.1.5 Performance Metric

The shape of the reagent coverage zone is used as the performance metric to evaluate the dipole system as a potential delivery tool. Different means of assessing this coverage zone are used for systems with and without a regional groundwater flow gradient. For systems without a regional hydraulic head gradient, only the coverage area is used, since the coverage zone is radially symmetric around the dipole/single well. Otherwise (ambient flow is not zero), the impact of ambient flow on the delivery performance will be assessed by comparing the shape of the coverage area with and without ambient flow influence. For each simulation, particles are released from the source chamber or well cylindrical face to delineate the dipole or single well coverage area.

2.2 Results and Discussion

Figures 2.3(a) and 2.3(b) show the coverage area of the dipole system and single well for the base case respectively. Flow from the upper chamber circulates to the lower chamber. The injected solution that is extracted out of the lower chamber (red flow lines in Figure 2.3 (a)) is called the captured flow. The percentage of captured flow, which is represented by the fraction of particles that are captured at the extraction chamber, increases over time. Same with horizontal dipole recirculation wells, after certain amount of the released reagent is captured, the dipole well system is stopped to avoid long time steady-state operation. During the preliminary testing, a trade-off occurs after roughly 30%~40% of captured flow (base case) is reached. After 40% of flow captured, the increase rate in the captured flow decreases considerably. To keep the amount of captured flow as a constant for the purposes of the

following sensitivity analysis, this investigation focuses on the coverage area evolution before 30% of injected flow is captured.

The arrival time distribution for the base case at the extraction chamber is shown in Figure 2.4. For this model configuration, it takes 0.9 days to capture 30% (36 out of 120) of the released particles. Since the coverage area without ambient flow is radially symmetric around the well (Figure 2.3), the following sensitivity analysis focuses on the geometry of the half coverage area (except for the ambient flow case) within 0.9 days. This allows for direct visual comparison between the base case and perturbed model scenarios.

Figure 2.5(a) illustrates the difference between coverage areas for the base case dipole and single well for the same injection rate, Q, (i.e., with the same injection costs). At the end of 0.9 days, the single well coverage area spans 2.64 m^2 in the vertical direction, which is 0.85 m^2 larger than the vertical extent of dipole coverage area. This is because the flow in a dipole system starts at the upper chamber and eventually is captured at the lower chamber. Therefore, the vertical extent of the dipole coverage area is limited by extraction at the lower chamber (Figure 2.3(a)). In contrast, the single well coverage area steadily increases, and the total mass of reagent in the system will also steadily increase. Horizontally, the dipole system covers a larger distance than the single well because of the different injection strengths, defined as the injection rate per vertical unit length along the chamber or well cylindrical face (6.67 m^2/d for the dipole and 1.33 m^2/d for the single well). A higher pumping strength leads to a higher horizontal velocity near the injection well screen, and correspondingly a larger horizontal component of the coverage area.

Within the first 0.9 days, the single well covers a larger area than the dipole system (3.44 m^2 for single well and 2.08 m^2 for dipole). As expected, the coverage area for the single well increases considerably faster beyond 0.9 days than the dipole well. Figure 2.6 shows the evolution of the coverage area and coverage volume for the dipole and single well. It is clear from this figure that in a homogeneous aquifer without regional flow, the single well outperforms the dipole system in terms of coverage volume. Because of the recirculation, the behaviour of the dipole system simply cannot distribute reagent to a large enough area to compete with the single well.

2.2.1 Ambient Groundwater Flow

Ambient flow will influence the travel distance and coverage area of the injected reagents (Figure 2.7). No matter how small the ambient flow is there will be some impact on the coverage area. In Figure 2.7(a), the ambient Darcy flux is 0.01m/d and the shape of coverage area along the plane parallel to the ambient flow seems to be symmetric around the well. In this case, the impact of ambient flow on dipole behavior is subtle. When the ambient flow rate is higher (Figure 2.7(b), q = 0.1 m/d), the shape of the coverage area is significantly changed, and quite asymmetric. A critical question, then, is whether (and when) we can neglect the influence of ambient flow during the design of dipole systems.

Regional groundwater flow is along the negative x-axis (Figure 2.5(b) and Figure 2.5(c)). Only the half coverage area down gradient of the well is depicted (see Figure 2.7(a)). It was found in preliminary simulations that ambient flow changes the shape of the down gradient half coverage area (DCA) more than up gradient half coverage area (Figure 2.7). Comparing the DCA in the base case (no ambient flow) with the result of the ambient flow case at 0.9

days (Darcy flux of ambient flow q = 0.03 m/d; Figure 2.5(b)), there is 5.8% increase in the DCA. Additional simulations (not shown) indicate that the DCA changes 2.7% and the single well coverage area changes 2.3% with ambient Darcy flux of q = 0.01m/d. As expected, the difference becomes larger when the magnitude of ambient flow increases. The ratio q/Q determines how much the influence the ambient flow has on the shape of the DCA. From these results when the ambient Darcy flux is less than 0.01m/d, which equals $q/Q < 0.005m^{-2}$, we may neglect the influence of ambient flow rate on the dipole and single well delivery performance (difference is less than 3% for both single well and dipole).

2.2.2 Influence of Chamber and Central Packer Length

The chamber length and the central packer length are important parameters in the design of a dipole system, and the correct selection of both impacts on the dipole performance in terms of the coverage area. To investigate the dipole behavior in response to variations in chamber length (2Δ), the base case of $2\Delta = 0.3$ m was perturbed to 0.5 m and 0.1 m, while keeping the packer length fixed at D = 0.5 m. A second set of tests perturbed the central packer length (from D = 0.7 to 0.5 and 0.9 m), while keeping the chamber length fixed at $2\Delta = 0.3$ m. Figure 2.5(d) and Figure 2.5(e) depict the change in coverage area with chamber length. Figure 2.5(f) and Figure 2.5(g) depict how the geometry of coverage area changes with the central packer length. As the dipole chamber length or central packer length increases, the dipole shoulder, defined as the distance between the centers of two chambers (Figure 2.2), increases as well. The above observation implies that dipole systems with a long dipole shoulder length will provide a better delivery than systems with a small dipole shoulder length, no matter whether this is due to an increase in chamber length or central packer length. The

circulated dipole flow sweeps larger area when the dipole shoulder length (the distance between the centers of the two chambers) increases.

2.2.3 Pumping Rate

As we can see in Figure 2.5(h) and Figure 2.5(i), the coverage areas become larger with an increase in pumping rate. As expected, injecting a reagent solution at a higher pumping rate can deliver the solution to a larger area than injecting reagents solution at a low flow rate at the same time due to the higher velocity of flow around the well.

2.3 Conclusion

Based on the above testing, it is clear that in homogeneous aquifers, ambient flow rate, chamber length, packer length, as well as pumping rate all exert influence on dipole performance. The above results indicate that, when installed in a single well with a standard well screen (approximately 1.5 m long), the dipole system sweeps a larger area when the chamber length or the central packer length increases. As expected, pumping rate influences the dipole performance in the same way: higher pumping rate helps dipole to sweep larger areas. By adjusting the dipole configuration (packer length and chamber length) and pumping rate, coverage areas of moderately different shape can be swept. However, the most critical result discovered here is that, in a homogeneous aquifer, a dipole cannot outperform the single well in terms of the coverage area. These results suggest that the single well injection approach is preferred over the more complex dipole configuration for reagent delivery in homogeneous aquifers under steady-state flow. However, this does not preclude the possibility that other aquifer configurations will not be better served with a dipole (or similar).

Because of this, Chapter 3 will address the detailed investigation of dipole performance vs. system configurations in homogeneous and heterogeneous aquifers.

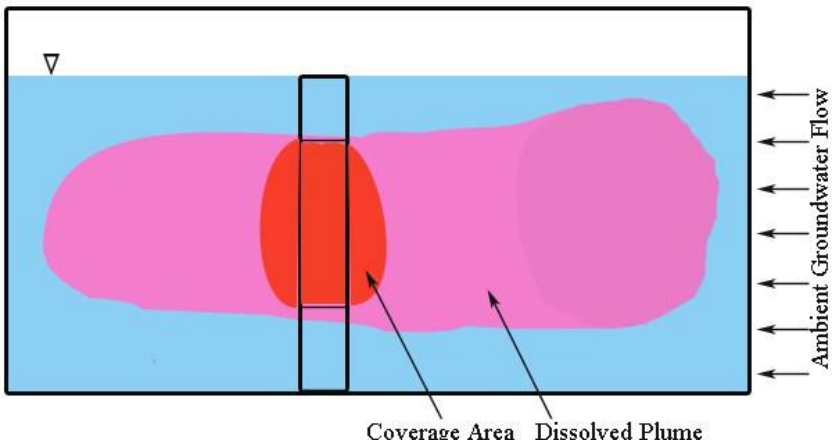

Figure 2.1. Schematic profile of the aquifer system showing a dipole injection well and a coverage area.

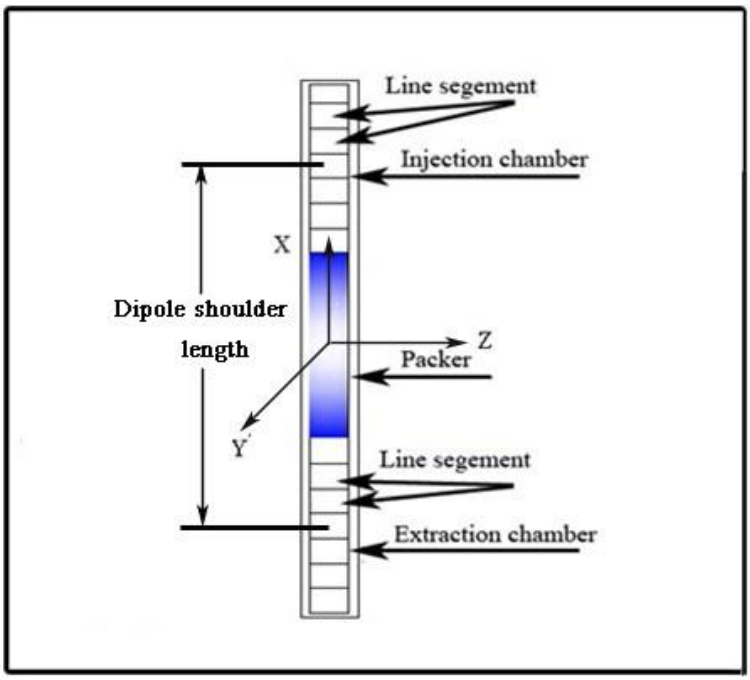

Figure 2.2. Line sinks/sources and line segments.

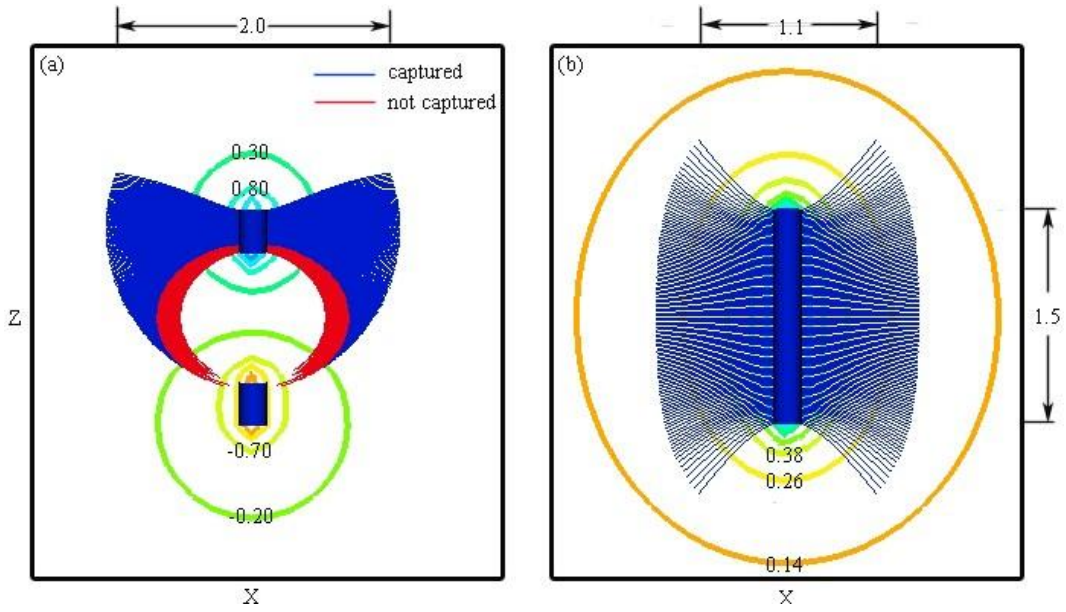

Figure 2.3. Coverage areas for (a) dipole base case, and (b) single well base case.

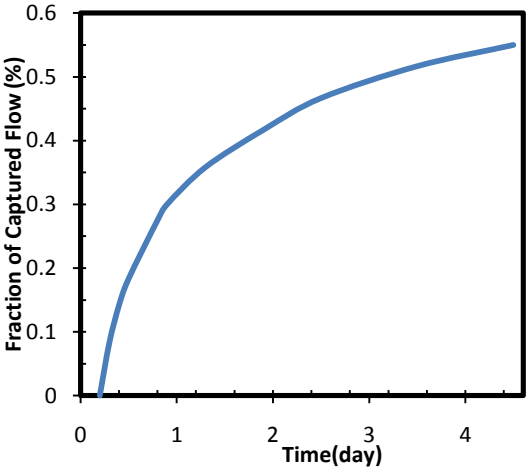

Figure 2.4. Particle arrival time distribution at the extraction chamber for the base case.

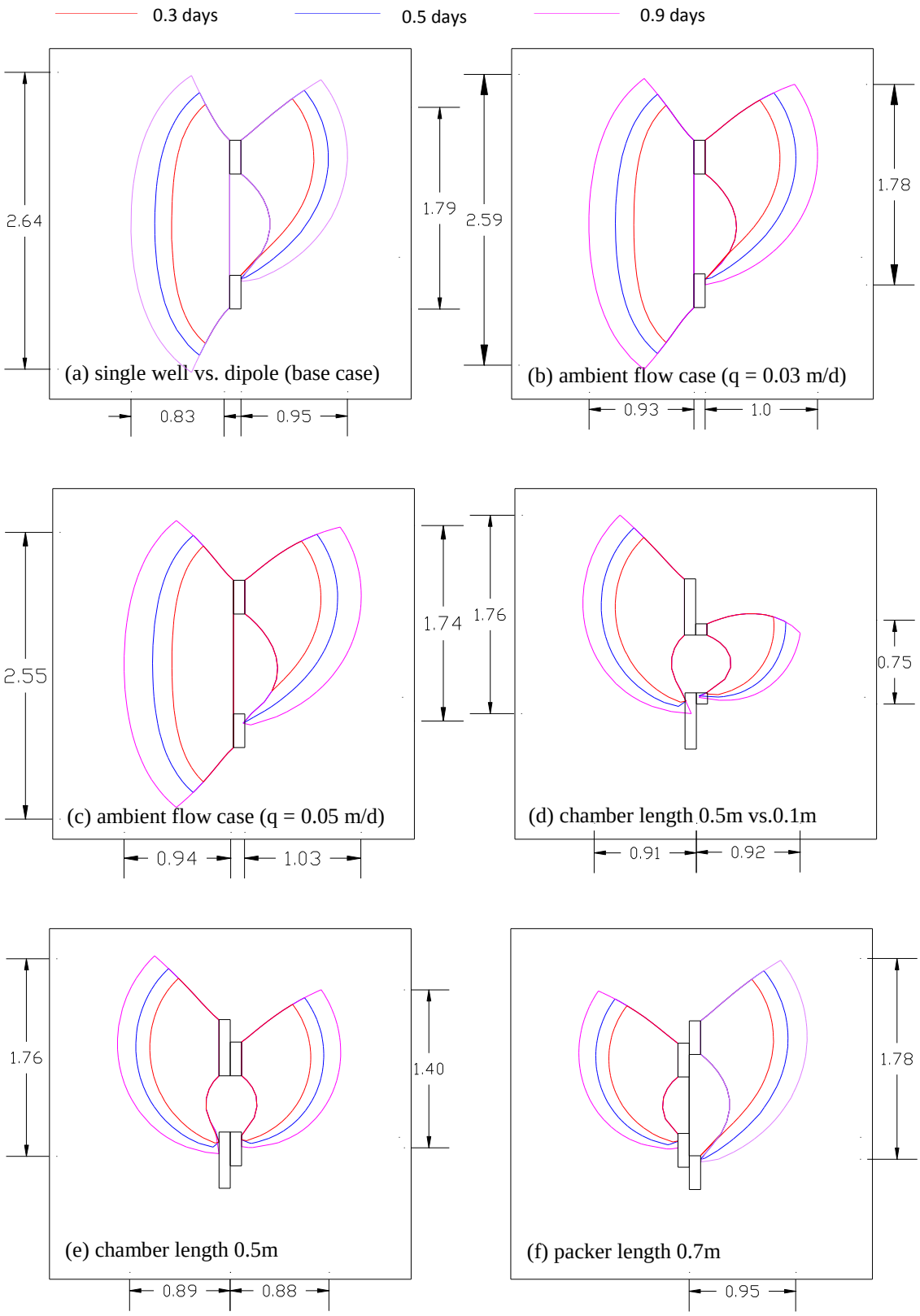
0.3 days
0.5 days
0.9 days
2.64
1.79
0.83
0.95
(a) single well vs. dipole (base case)
2.59
1.78
0.93
1.0
(b) ambient flow case (q = 0.03 m/d)
2.55
1.74
0.94
1.03
(c) ambient flow case (q = 0.05 m/d)
1.76
0.75
0.91
0.92
(d) chamber length 0.5m vs.0.1m
1.76
1.40
0.89
0.88
(e) chamber length 0.5m
1.78
0.95
(f) packer length 0.7m

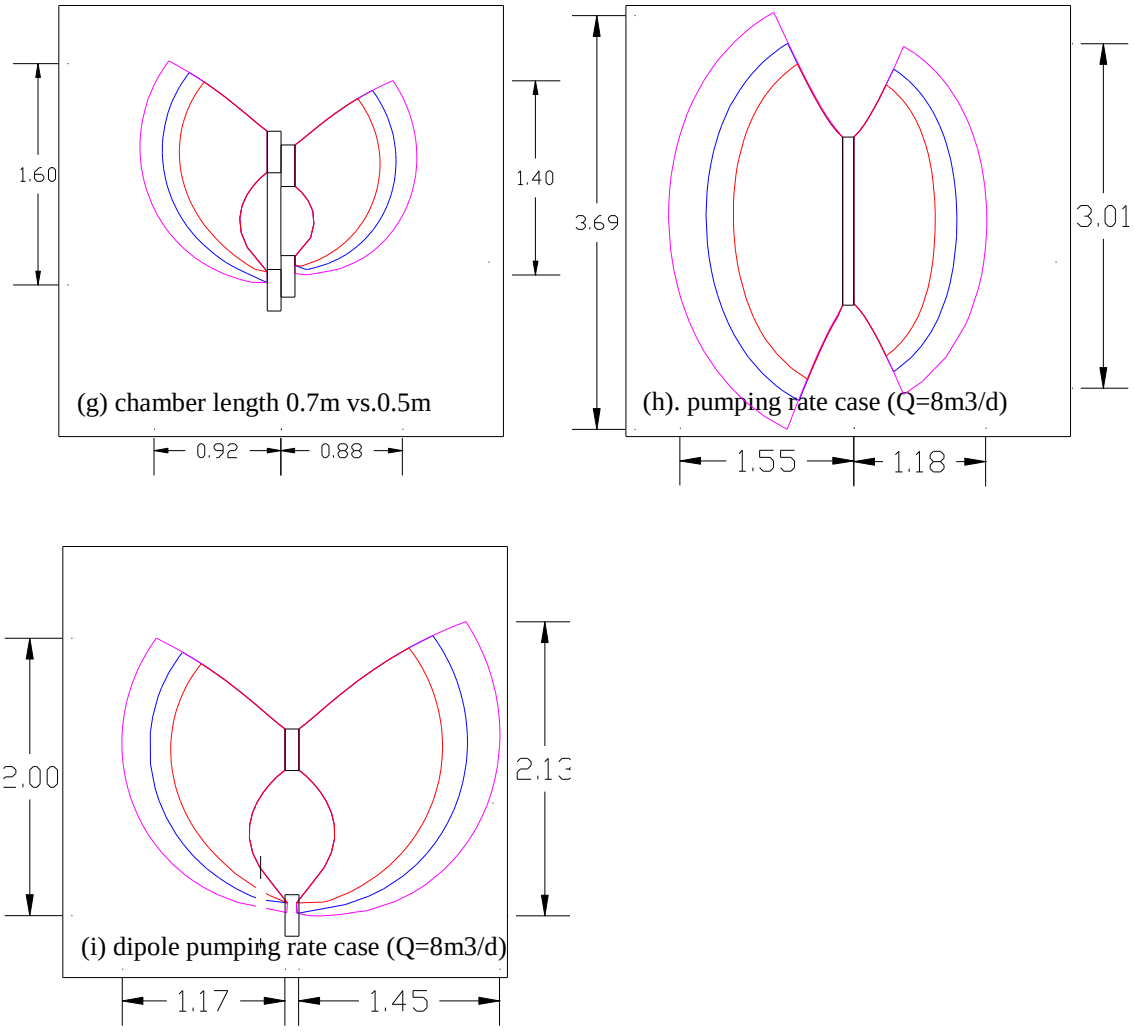

Figure 2.5. Coverage areas along the dipole/single well under various model configurations: (a) base case of dipole and single well; (b) ambient flow rate q=0.03m/d (dipole and single well); (c) ambient flow rate q=0.05m/d (dipole and single well); (d) chamber length (0.1m and 0.5m); (e) chamber length (0.3m and 0.5m); (f) packer length (0.5m and 0.7m); (g) packer length (0.5m and 0.9m); (h) injection rate Q=8m^3/d and Q=4m^3/d (single well); (i) injection rate Q=8m^3/d and Q=4m^3/d (dipole well).

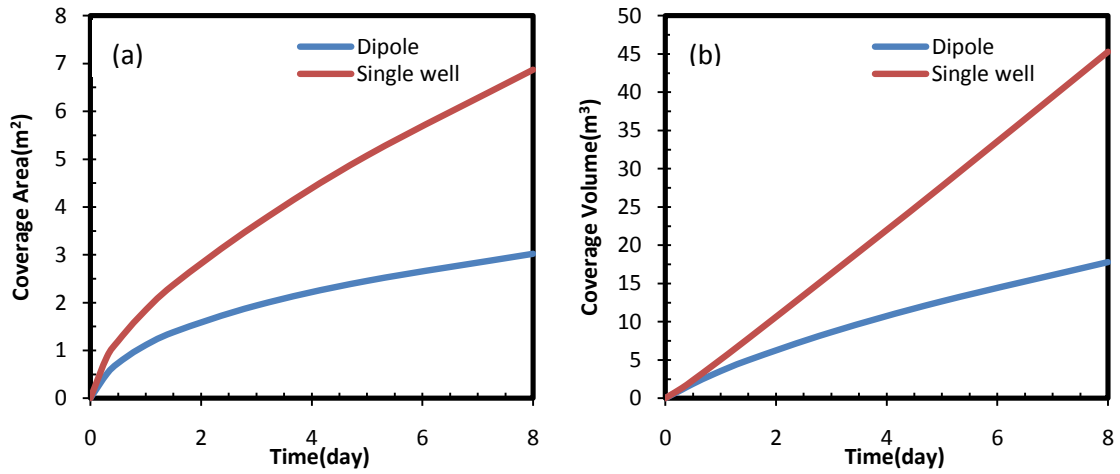

Figure 2.6. (a) Evolution of the coverage area for dipole and single well, and (b) swept volume of dipole and single well with time.

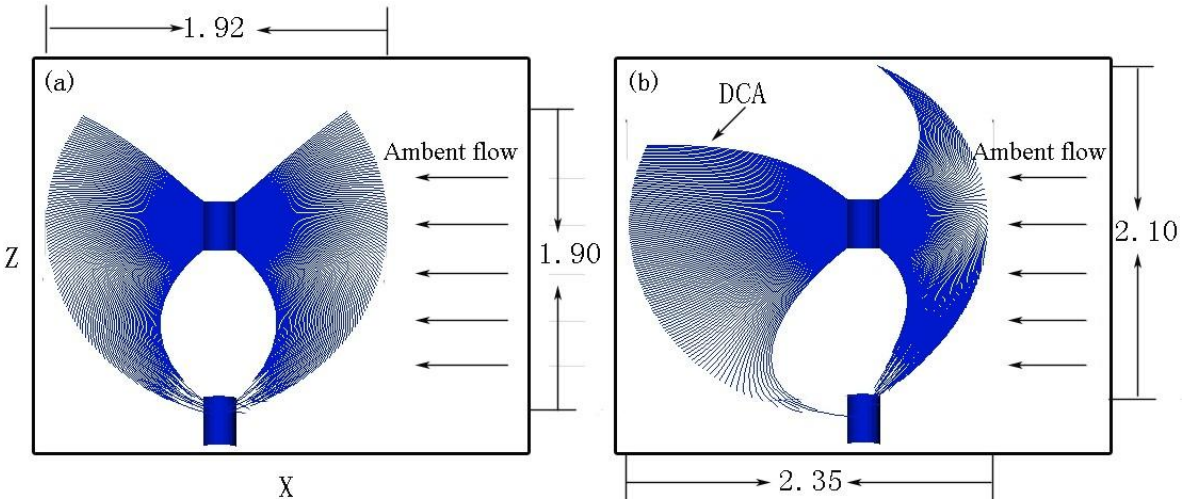

Figure 2.7 Coverage areas for ambient Darcy flux of (a) q=0.01 m/d, and (b) q=0.2m/d.

Table 2.1 Model input data for sensitivity analysis

SC	Delivery	2D(m)	2Δ(m)	Q(m^3/d)	q(m/d)
Base	Dipole	0.9	0.3	2.0	0.0
	SW	-	1.5	2.0	0.0
Ambient Flow	Dipole	0.9	0.3	2.0	0.03
	SW	-	1.5	2.0	0.03
	Dipole	0.9	0.3	2.0	0.05
	SW	-	1.5	2.0	0.05
Chamber length	Dipole	0.5	0.1	2.0	0.0
		0.5	0.5	2.0	0.0
Well spacing	Dipole	0.5	0.3	2.0	0.0
		0.7	0.3	2.0	0.0
Pumping rate	Dipole	0.9	0.3	3.0	0.0
		0.9	0.3	4.0	0.0
Porosity	Dipole	0.9	0.3	2.0	0.0
	SW	-	1.5	2.0	0.0
	Dipole	0.9	0.3	2.0	0.0
	SW	-	1.5	2.0	0.0

SW- single injection well;
SC-simulation case.

Chapter Three Performance Evaluation

3.1 Introduction

In this chapter, numerical simulations are used to investigate the transient behavior of the dipole system as it delivers reagent in both homogeneous and heterogeneous aquifers. Different dipole system configurations, injection rates, and hydraulic conductivity fields can influence the dipole delivery behavior. A sensitivity analysis is conducted to study the impact of selected parameters on the dipole system performance. The delivery capability of the dipole system is evaluated using the down gradient coverage area (Figure 3.1) along a plane orthogonal to the ambient groundwater flow direction. This down gradient coverage area is a quantitative surrogate to assess reagent delivery. Consistent with Chapter 2, a single well is also simulated for comparison purpose. The findings from this comparison will be used to discern situations where a dipole delivery system may be advantageous.

3.2 Methods

Advective particle tracking is used to delineate the down gradient coverage area of a dipole or a single well reagent injection system. The finite difference model MODFLOW-2000 (Harbaugh et al., 2000) is used to calculate the velocity field, and MODPATH (Pollock, 1994) is used to track a lattice of particle paths backward from the down gradient plane. The subset of backtracked particles which originate from the delivery well represent the reagent solution that can be delivered to the downstream plane.

3.2.1 Model Domain and Discretization

The selected model domain is 40 m × 40 m × 11 m along the x, y and z-axes, respectively (Figure 3.2). These spatial dimensions are large enough compared to the perturbations caused by the dipole or single well that the boundary conditions do not affect the flow solution near the well. This negligible boundary effect was verified with preliminary simulations (not reported here) for the flow rates and injection schedules tested (injection schedules will be covered in the following section). The spatial domain was discretized into 146 rows, 146 columns and 55 layers (Table 3.1). The hydraulic head gradient around both the dipole and single well is high relative to other zones in the domain, and therefore a finer resolution in this area was needed. Preliminary simulation results also indicated that the volume balance error (difference between inflow and outflow) was less than 1%.

3.2.2 Parameterization

The initial performance of a dipole delivery system is intended to be field tested at Canadian Force Base Borden, near Alliston, Ontario, Canada (Roos, 2008). For this reason, the initial hydraulic parameter values are based on the Borden aquifer properties. A uniform porosity value of 0.33 was used. The uniform aquifer specific storage of 0.001/m was referenced from Frind (1998).

In Chapter 2, the steady-state dipole behavior in a homogeneous aquifer was investigated. This homogeneous aquifer investigation will first be replicated for transient dipole flow (pulsed injection), and then extended to structured and randomly heterogeneous media (Figure 3.3 and Figure 3.4). For each aquifer configuration (homogeneous, structured, and randomly

heterogeneous), a different hydraulic conductivity field was used. For the homogeneous aquifer, the hydraulic conductivity (0.864 m/d) was uniform ($K_{xx} = K_{yy} = K_{zz}$).

The structured hydraulic conductivity field has a 0.1 m thick, lower hydraulic conductivity layer lying in the middle of the homogeneous aquifer, coincident with the center of the dipole central packer (Figure 3.3). The lower hydraulic conductivity was specified to be two orders of magnitude lower than the surrounding homogeneous medium (0.00864 m/d, which is a clean to silty sand (Prakash, 2004)).

For the randomly heterogeneous aquifer, the hydraulic conductivity is not uniform but follows a specified statistical structure, where the hydraulic conductivity is a spatially correlated random variable that satisfies a lognormal probability density function. For a statistical characterization, random generated fields were used in this study to assess the dipole performance in heterogeneous aquifers. These fields were generated using the geostatistical model - Random Field Generator (RFG) (Robin, 1993), which uses the Direct Fourier Transform Method to generate heterogeneous hydraulic conductivity distributions. These fields are used as the input hydraulic conductivity in MODFLOW-2000. Correlation length and variance are referenced from Sudicky (1986) (Table 3.2). Additional heterogeneous hydraulic conductivity fields were also generated with either higher variances to yield more heterogeneous conductivity fields, (i.e., Figure 3.4 (b)) or an altered correlation length. The investigation using heterogeneous fields will illustrate the delivery performance of the dipole or single well in response to different hydraulic conductivity distributions (Table 3.2).

3.2.3 Well Properties

Consistent with the steady-state dipole simulations, it is assumed that the single well dipole system uses a standard screen (approximate 1.5 m long). The chamber length and central packer length are therefore confined to the range [0.1, 0.5], and hence the constraint $4\Delta + D \leq 1.5$ m is satisfied naturally. The default dipole configuration, as with the steady-state case, has a 0.3 m chamber length and 0.5 m central packer length. Injection rates used in the sensitivity analysis (2, 4, 6 and 8 m^3/d) are identical with the steady-state simulations. All parameter values used for the sensitivity analysis are outlined in Appendix B. To assess the impact of the hydraulic conductivity distribution on dipole behaviour, the dipole well has the same default configuration for the structured hydraulic conductivity fields and randomly heterogeneous fields as used for the homogeneous case.

3.2.4 Boundary Conditions

Constant hydraulic heads are applied to the up gradient and down gradient boundaries of the domain (with the constant hydraulic head values set to replicate an ambient flow velocity of 0.1 m/d). No-flow boundaries are applied at the top and bottom of the domain. Each layer in the domain (total 55 layers) is unconfined.

3.2.5 Injection Schedule

In order to perform the transient simulations discussed here, a reasonable reagent injection schedule for this system needs to be identified. Preliminary simulations of the dipole base case showed that the rate of increase in coverage area decreases over time up until roughly 0.4 days (after 0.4 days, the rate of increase in coverage area is approximately constant, and

smaller than the rate at t < 0.4 days). The rate of the captured flow decreases considerably after about 30% ~ 40% injected flow returns. The fraction of the captured flow at the end of the first injection cycle is close to 40% if the pulsed injection time is 0.4 days (37% of the flow is captured after the first injection cycle and the fraction will be larger than 37% at the end of the second injection cycle determined by the specific injection schedule). Hence, to limit the volume of reagent captured, a threshold of 40% of the captured flow was set after two injection cycles. Moreover, the interval between the two injection cycles should be short or else the coverage zone is not continuous, and will be separated by ambient groundwater (Figure 3.1). Preliminary model results show that if the injection is on for 0.2 days and off for 1.8 days sequentially, the coverage areas of the two sequential injection cycles overlap with each other (i.e., the coverage area is continuous) and 38.2% of flow is captured at the end of the two injection cycles. All of these behavioral traits are desirable. This pulsed injection schedule (on for 0.2 days and off for 1.8 days) was therefore selected for the investigation at injection rate of 2 m^3/d. When higher injection rates (i.e., 4, 6 and 8 m^3/d) are adopted, the same injection schedule is applied to investigate the impact of higher injection rates in conjunction with the system configuration parameters.

Preliminary simulation results showed that in the randomly heterogeneous aquifer (Heterogeneous Field #1 in Table 3.2) with the same injection cycle, about 21.7% of flow is captured at the end of the second injection cycle. Therefore, the same injection schedule is adopted for the randomly heterogeneous K field simulations.

The appropriate time and location of the monitoring plane for the structured hydraulic conductivity field will necessarily have to differ from the homogenous case. Due to the

presence of the lower hydraulic conductivity layer, the hydraulic connection between the injection and extraction chamber decreases. Therefore, the arrival time of the captured flow increases correspondingly. Figure 3.5 shows the relationship between the fraction of captured flow and the arrival time at various injection rates. For example, only about 19% of flow is captured at an injection rate of 2 m^3/d after 9 days, as compared to 17% after 0.2 days for the homogeneous case. At an injection rate of 2 m^3/d, after roughly 19% of injected flow is captured, the increase in the amount of captured flow slows down considerably. The path lines along the plane of the well at various injection rates are shown in Figure 3.6 when about 19% of flow is captured. The overall shape of the coverage area along the plane of the well is similar but the corresponding arrival time is different (9.0 days, 5 days, 4 days and 1.8 days for Q = 2, 4, 6 and 8 m^3/d respectively). It is desirable to have the duration of the injection cycles short to avoid the long and steady-state operation of dipole system (e.g., 4-day injection). For a given amount of captured flow (i.e., 19%) at the injection rates of 2, 4, 6 and 8 m^3/d, the operational time decreases dramatically as the injection rate increases. Therefore, we select 8 m^3/d as the pulsed injection rate in the structured field (as mentioned, injection rates larger than 8 m^3/d are not considered in this research). The injection-off period of 1.8 days is referenced from the homogeneous injection schedule.

3.2.6 Performance Metrics

The coverage area around the injection well cannot be used as the performance metric for the simulations performed in this chapter because the coverage zone is not radially symmetric to the well. Therefore, the downstream coverage area is the only performance metric used to characterize the delivery capability of a dipole or single well.

To select a reasonable monitoring plane and a reference time to monitor the downstream coverage area, an understanding of the impact of the pulse injection on the dipole flow paths is required. Figure 3.7 shows the path lines for the homogeneous case at the end of multiple injection cycles. When the reagent is transported further away from the well (i.e. past the downstream plane 1.9 m away from the well or x = 18.1 m in the spatial domain), the impact of dipole pulsed injection frequency is less apparent (i.e., lines become gradually flat down gradient, as can be seen in Figure 3.7(f)). However, if the downstream plane is too close to the well and within the coverage area at the end of the first injection cycle (e.g., 0.1 m away down gradient of the well), the influence of pulsed injection cycles is not captured. The downstream coverage should be monitored at a plane where the influence of the pulsed injection is dominant. Therefore, the downstream plane 0.9 m away from well (x = 19.1 m) was selected to monitor the dipole and single well performance (Figure 3.7 (f)).

For the homogeneous base case, it was determined that after the eighth injection cycle the coverage area along the plane aligned with ambient flow reached a pseudo steady-state that is defined as a state when the coverage area is only extending down gradient (Figure 3.7(e) and Figure 3.7(f)). Therefore, the downstream coverage area is monitored at the end of the eighth injection cycle.

The location of the downstream monitoring plane and the selection of a monitoring time will have to be altered for a specific heterogeneous hydraulic conductivity field since it is not reasonable to set a uniform downstream monitoring plane and time for all the heterogeneous hydraulic conductivity fields to be investigated. Specific information about the downstream monitoring location and the time in each hydraulic conductivity field (not for the

homogeneous aquifer) are discussed where and when appropriate in section 3.2 below. However, the justification of the downstream monitoring plane and time selection is consistent with the homogenous simulation.

3.3 Results and Discussion

3.3.1 Homogeneous Hydraulic Conductivity Fields

In this section, the influence of each parameter on the performance of the dipole delivery system is assessed for the homogeneous aquifer. For all aquifer systems, the dipole delivery performance is evaluated in comparison with the single well.

Figure 3.8 shows the single well path lines under pulsed injection aligned with the ambient flow direction. The uniform spatial flow distribution of single well covers an apparently larger area than the dipole well because the vertical circulated flow confines the increase in the dipole coverage area (Figures 3.7 and 3.8). Figure 3.9 shows that the single well downstream coverage area is apparently larger than that of dipole. The vertical extent of the dipole downstream coverage area is smaller than that of single well downstream coverage area (0.6 m difference) consistent with the observation of the coverage area delineated by the path lines along the well.

The various dipole configurations tested, together with the sensitivity analysis results, are included in Appendix B. According to these results, with configuration $2\Delta = 0.5$ m, $D = 0.5$ m, dipole can produce a similar downstream coverage area compared to a single well at an injection rate 2 m^3/d (the dipole downstream coverage area is 3.40 m^2 and the single well

downstream coverage area is 3.23 m^2). As expected, both the dipole well and the single well coverage area increases with a higher injection rate, consistent with the findings in Chapter 2. The dependence of downstream coverage area on system parameters is shown in Figure 3.10. Figures 3.10 (a) - (d) show that the relationships between log-A (where A is the downstream coverage area) and the log of the individual system parameters (2Δ, D, L and Q) appear to follow linear trends. Within the constraint that $4\Delta + D \leq 1.5$ m, increasing any of the four perturbed parameters (2Δ, D, L, and Q) leads to an increase in the downstream coverage area, consistent with the observation in Chapter 2. The relationship of log-A vs. log-L also follows a linear relationship and captures the effect of chamber length and central packer length as a single factor on the downstream coverage area. Therefore, it is hypothesized that L is the characteristic length of dipole delivery performance rather than just the chamber length or packer length.

Figures 3.10(e) - (f) show the trend between the log-A and log-t_p (pulsed injection time), and log-A and log-(Qt_p) respectively. Keeping one of them fixed and varying the other, Q or t_p influences the downstream coverage area uniquely, but Q and t_p combined together are actually related to the injection cost, which is assumed to be proportional to the injected volume of reagent Qt_p (shown in Figure 3.10(f)). The relationship of log-A vs. log-(Qt_p) explains the impact of Q and t_p as a single factor on A. Therefore, the characteristic terms L and Qt_p can be used to normalize the results by assuming that:

$$\frac{A}{L^2} \sim f\left(\frac{Qt_p}{L^3}\right) \tag{3.1}$$

where t_p is the pulsed injection time [T], Q is the injection rate [L^3/T], L is the dipole shoulder length [L], and A is the downstream coverage area [L^2]. These particular units were chosen in order to express the results in terms of dimensionless quantities.

Figure 3.11 shows the scatter plot of Eq. (3.1) and the linear relationship given by:

$$\log\left(\frac{A}{L^2}\right) = 0.49 \log\left(\frac{Qt_p}{L^3}\right) + 0.89 \qquad (3.2)$$

with the coefficient of multiple determination R^2=0.99.

Eq.(3.2) can be rearranged to yield the following expression for the downstream coverage area to:

$$A \approx 7.75 \sqrt{Qt_p L} \qquad (3.3)$$

Note that Eq. (3.3) is based on the finite number of simulations and is only valid for $Q \leq 8$ m^3/d, and $4\Delta + D \leq 1.5$m.

Based on the observations associated with Figure 3.10(d), when the shoulder length increases the dipole delivery performance can be improved. Therefore, for the extreme dipole configuration situation and using Eq. (3.3) (t_p = 0.2 d; Q = 2 m^3/d; 2Δ = 0.1 m; D = 1.3 m) the dipole downstream coverage area $A \approx 4.10$ m^2. This value is 25% larger than the single well coverage area of 3.28 m^2. However, when the injection cost is larger (e.g., Qt_p = 0.8 m^3) the single well can outperform the dipole well (see Appendix B).

3.3.2 Structured Hydraulic Conductivity Field

The presence of a lower hydraulic conductivity layer separating the dipole chambers is expected to influence the efficiency of the dipole system, and this has been simulated using

models similar to those evaluated above. Figure 3.12 shows the dipole path lines along the well plane in the structured field. The horizontal extent of the dipole coverage area is much larger than the vertical extent and thus more mass of injected reagent is located above the lower K layer. This is because the presence of the lower K layer decreases the dipole flow connection and thus the vertical velocity is smaller than the horizontal velocity. In Figure 3.13, the path lines originating from the single well are similar to those in the homogeneous aquifer (Figure 3.8) except that there is an unswept area coincident with the lower hydraulic conductivity layer because the single well flow cannot force the injected solution to travel through this layer. Figures 3.14(a) - (b) shows the downstream coverage area (3.0 m away from the well) for the dipole and single well respectively. Although apparently the overall downstream coverage area of the single injection well is much larger than the dipole, the dipole well can distribute reagent below the lower hydraulic conductivity layer.

When the location of the lower hydraulic conductivity layer is shifted higher/lower between the two chambers of a dipole well, the mass of injected reagent distributed beneath the lower K layer increases/decreases correspondingly. When the distance of the upper chamber and the lower K layer becomes smaller (i.e., the lower K layer shifting up), the time that it takes for the injected reagent to reach the lower K layer is shorter as well. Therefore, at a given amount of time the mass of the reagent that reaches and travels through the lower K layer increases.

To further investigate the impact of a lower K layer on the performance of the dipole delivery system the thickness and the hydraulic conductivity of the lower K layer were increased by a factor of two (0.2 m thick and K = 0.0173 m/d). Surprisingly the path lines for this altered lower K layer (Figures 3.15 and 3.16) are similar to the initial case (Figures 3.12 and

3.13). The shape of downstream coverage areas is shown in Figures 3.14(c) - (d) for both the dipole and single well respectively. Due to the increased thickness of the lower K layer, the downstream coverage area for the single well is less than that determined for the initial case. The downstream coverage area for the dipole well is similar in both structured fields (Figure 3.14(a) vs. Figure 3.14(c)). It is hypothesized that when multiple layers of lower hydraulic conductivities are present the downstream coverage area for the single well will eventually decreases to be smaller than that of dipole well. This hypothesis will be tested in the next section where multiple lenses of lower hydraulic conductivity are present in the synthesised heterogeneous aquifers.

3.3.3 Heterogeneous Hydraulic Conductivity Fields

Based on the observations noted in Section 3.2.2, it is expected that the dipole well will outperform the single well in some heterogeneous aquifers. Therefore, the performance of the injection wells is first investigated in a randomly heterogeneous field (Heterogeneous Field #1) that has the same hydraulic conductivity structure as the Borden aquifer. Heterogeneous Field #2 and #3 have the same structure as Heterogeneous Field #1 but with larger variances (0.5 and 1.0 log-m^2/d^2 respectively) and hence are more heterogeneous. The difference in the delivery performance in the three randomly heterogeneous aquifers will shed light on the impact that an increase in the degree of heterogeneity will have on the dipole and single well behaviour.

To investigate the delivery performance in other possible heterogeneous aquifers, four other randomly heterogeneous fields were generated. Randomly heterogeneous fields with a smaller x-y correlation lengths (1.4, 0.7 and 0.1 m for Heterogeneous Field #4, #5 and #6 respectively)

are used to assess the impact of the horizontal scale of bedding planes on the performance of the dipole and single injection wells. The z-correlation length (0.12 m), which reflects the thickness of hydraulic conductivity lenses, is fixed due to the small dipole shoulder length of 0.4 m. If the thickness of a hydraulic conductivity lens is close to 0.4 m or even larger, the dipole well will reside within a relatively homogenous medium and thus the influence of the layers of different K is minimized. Note that only one model realization was used for each set of geostatistical parameters.

Heterogeneous Field #1

As shown in Figure 3.4(a), Heterogeneous Field #1 has distinct locations of lower hydraulic conductivity layers. Based on the hypothesis outlined in Section 3.2.2, the dipole and single well performance operating in locations with the presence of different hydraulic conductivity lenses will be monitored to observe the resultant behaviour. However, as the initial step path lines will be used to show the distribution of the injected solution.

Figures 3.17 and 3.18 show the path lines originating from the dipole system and single well in Heterogeneous Field #1, tracked along the plane aligned with the ambient flow direction. The travel distance of the injected reagents varies along different layers in the heterogeneous aquifer. As expected, in the high permeable areas (such as the one in the lower half of these images), the travel distance is longer than that in low permeable areas. The distribution of the injected reagent is relative homogeneous around the single well though within a heterogeneous aquifer.

If the location of the injection is shifted to the front of the coverage area at x = 17.4 m (Location A) to monitor the delivery performance, the shape of the coverage area delineated by path lines is changed. Figures 3.19 and 3.20 show the path lines of dipole well and single well respectively at Location A. Single well path lines are much shorter along the horizontal layer between z = 4.4 m and z = 5.0 m than those at other layers, while dipole well path lines do not display a similar phenomenon. As expected, the high permeable zones dominant reagent flow away from the single well, leaving the low permeable zones unswept. The dipole well is efficient in sweeping the low permeable downstream area. The downstream coverage area (about 0.9 m away from well) for the single well and dipole well are depicted in Figure 3.21 and provide a vivid picture of the delivery difference between the two methods. There is about a 20% difference in downstream coverage area between dipole and single well (3.43 m^2 and 2.86 m^2 respectively).

Heterogeneous Field #2 and #3

Figures 3.22(a) - (f) show the path lines of the dipole and single well in Heterogeneous Fields #1 - 3 at the end of the eighth injection cycle respectively when the dipole coverage areas have reached a pseudo steady-state. The horizontal extent of dipole coverage area delineated by the path lines is smaller than that of the single well, consistent with the observation in Sections 3.2.1 and 3.2.2. The distribution of the injected reagent for either the single well or dipole well is different in each randomly generated hydraulic conductivity field. However, for the single well, the travel distance of the injected reagent is longer in high permeable areas than that in low permeable areas. For the dipole well the path lines in Heterogeneous Fields #1 and #2 the travel distance is not apparently influenced by the layered heterogeneous

hydraulic conductivity. Figure 3.22(e) shows that in Heterogeneous Field #3 the injected reagent by the dipole well has a similar distribution with that produced by a single well in Figure 3.22(f) (i.e., along the layers between about 5.0 m and 7.0 m, the travel distance of the injected reagent is shorter than that along the other layers). Only comparing the coverage area along the x-z plane is not sufficient to identify the impact of heterogeneity on the delivery performance of the dipole or single well. The downstream coverage area along the y-z plane is at the same time used to determine how the dipole and single wells respond to the increased degree of heterogeneity. Figure 3.23 shows the downstream coverage area (0.9 m away from well downstream) of dipole and single wells in Heterogeneous Field #2 while Figure 3.24 shows the downstream coverage area (1.4 m away from well downstream) for the dipole and single wells in Heterogeneous Field #3. The downstream coverage area for the dipole well is apparently larger than that of single well in Heterogeneous Field #2. However, the overall shape of the downstream coverage area for the dipole well in Heterogeneous Field #3 is not as smooth as that in Heterogeneous Fields #1 and #2 due to the increased degree of heterogeneity (Figures 3.21, 3.23 and 3.24). The performance of dipole delivery in Heterogeneous Field #3 is not as good as that in Heterogeneous Fields #1 and #2 based on the distribution of path lines and overall shape of downstream coverage area. Moreover, the advantage of delivery performance of the dipole well over a single well is not apparent in Heterogeneous Field #3.

Heterogeneous Field #4, #5, #6 and #7

Figures 3.25(a) - (h) show the path lines originating from the injection well in Heterogeneous Fields #4, #5, #6 and #7 at the end of the eighth injection cycle when the coverage areas of

dipole well has reached a pseudo steady-state. The impact of heterogeneity on the single well delivery performance is similar in Heterogeneous Fields #1 - #5 (the travel distance of the injected reagent is non-uniform along the different layers). In Heterogeneous Fields #1, #2, #4 and #5, the impact of heterogeneity on the dipole path lines is not as apparent as that on single well path lines because the circulated dipole flow can overcome the lenses of contrasting hydraulic conductivities within a certain degree of heterogeneity (e.g., variance of 0.3 log-m^2/d^2 in Heterogeneity Field #1). The path lines for a single well in Heterogeneous Field #6 show that the distribution of the injected reagent is close to uniform. The downstream coverage area (0.9 m down gradient of the well) also indicates the same phenomenon; the overall shape of single well downstream coverage area is close to smooth in Heterogeneous Field #6 (λ_{xy} = 0.1 m) in Figure 3.26(b) since the impact of heterogeneity is small on the performance of single well. Keeping the structure of Heterogeneity Field #6 fixed and increasing the variance of hydraulic conductivity as in Heterogeneous Field #7 (0.5 log-m^2/d^2), the performance of single well is similar in both randomly heterogeneous hydraulic conductivity fields (Heterogeneous Fields #6 and #7) according to the distribution of the injected reagent. The downstream coverage areas for the single well in both heterogeneous fields (Heterogeneous Fields #6 and #7) also show that the impact of heterogeneity on delivery performance is small (Figures 3.26 (b) and 3.26(d)). This is possibly because when the size of the bedding plane becomes small (i.e., 0.1 m), the single well can force the injected solution to travel through lower hydraulic conductivity lenses. According to the dipole path lines and downstream coverage area (Figures 3.26(a) and 3.26(c)) in Heterogeneous Fields #4 - #6, there is no apparent influence of heterogeneity on dipole well performance but in

Heterogeneous Field #7, there is a small unswept area 2.0 m away from dipole well downstream. This is possibly because the effect of dipole pulsing injection is small and hence the injected solution cannot sweep that lower K area. The overall shape of dipole downstream coverage area indicates that the distribution of the injected reagent is close to smooth and thus the performance of dipole is not apparently influenced by hydraulic conductivity distribution in Heterogeneous Fields #6 and #7 as well (Figures 3.26(a) and Figure 3,26(c)).

Based on the above findings for these selected heterogeneous hydraulic conductivity fields, the impact of the structure of randomly heterogeneous K fields on the dipole well performance is not as apparent as that on a single well but the degree of heterogeneity does influence the dipole delivery performance (i.e., Heterogeneous Field #3). When the x-y correlation length decreases to 0.1 m, a single well injection can perform quite well with little influence of heterogeneity even if the degree of the K increases (i.e., variance increases from 0.3 to 0.5 log m^2/d^2 in Heterogeneous Fields #6 and #7).

3.4 Conclusions

Dipole performance is determined by the system configuration (dipole packer length, chamber length, and injection cost Qt_p) and the physical properties of the aquifer. In both homogeneous and heterogeneous aquifers, dipole delivery is efficient for low injection volumes (Qt_p), but at a higher injection cost (i.e., >4 m^3/d for a 0.2 day pulse duration), the downstream coverage area of dipole will not increase as fast as that of a single well in the same time frame. The main reason for this inequity is that the dipole circulation flow confines the vertical extent of the downstream coverage area. It is for this reason that dipole performance is more affected

by the shoulder length (the total distance between chamber ends) than by the individual lengths of the chamber and central packer.

The investigation in the structured and heterogeneous K fields shows that the distribution of hydraulic conductivity has a more pronounced and deleterious effect upon the performance of the single well than the dipole well. The presence of a lower hydraulic conductivity layer in structured K fields will decrease the vertical flow velocity as well as the vertical extent of the dipole downstream coverage area. However, the dipole well is more effective in sweeping the lower hydraulic conductivity layer than the single well due to the predominantly vertical flow in the lower hydraulic conductivity layer. As the thickness of a lower hydraulic conductivity layer increases, single well downstream coverage area decreases correspondingly but the dipole well downstream coverage area is not apparently affected.

Based on this observation, the dipole well is expected to outperform the single well in the synthesised heterogeneous fields where lenses of contrasting hydraulic conductivities are present. Single well performance is apparently influenced by the structure of heterogeneous K fields and thus some lower permeable areas are unswept. However, if the x-y correlation length becomes as small as 0.1 m, the impact of heterogeneity on the performance of the single well is correspondingly small. The response of dipole well to the heterogeneity is subtle if the degree of heterogeneity is mild (e.g., Heterogeneous Field #1), otherwise the performance of dipole delivery may decrease (e.g., Heterogeneous Field #3). The advantage of dipole well over single well delivery is not apparent either in a highly heterogeneous hydraulic conductivity field (e.g., Heterogeneous Field #3) or in a hydraulic conductivity field where the horizontal extent of the bedding plane is small (e.g., Heterogeneous Field #6).

Hence, in these cases (e.g., Heterogeneous Fields #3 and #6) the single well is a preferred delivery method due to its simple configuration.

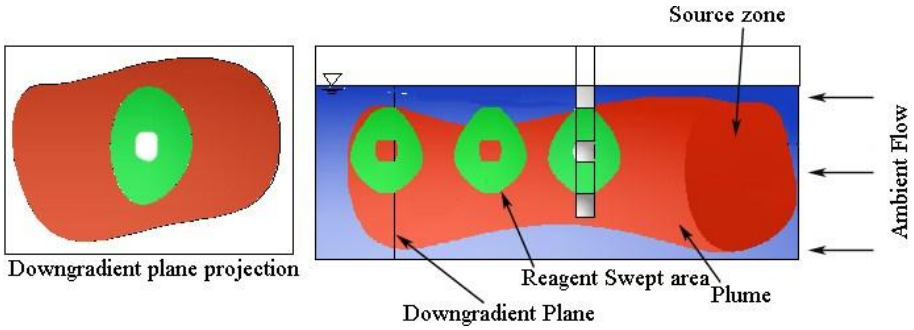

Figure 3.1. Coverage area, plume profile, and down gradient plane.

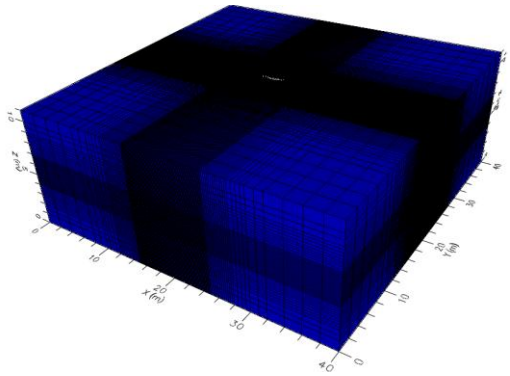

Figure 3.2. Three dimensional model domain and discretization.

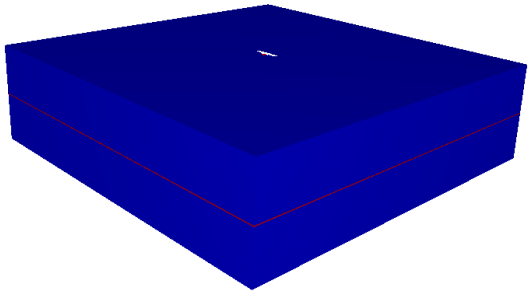

Figure 3.3. Structured hydraulic conductivity field.

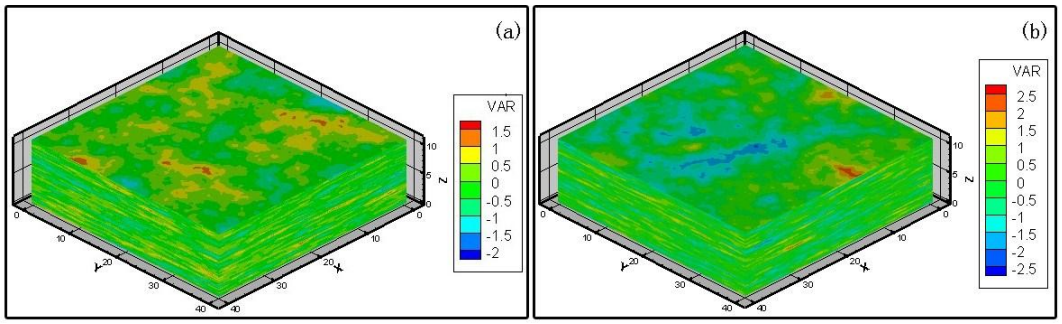

Figure 3.4.Randomly heterogeneous hydraulic conductivity field: (a) #1; (b) #2.

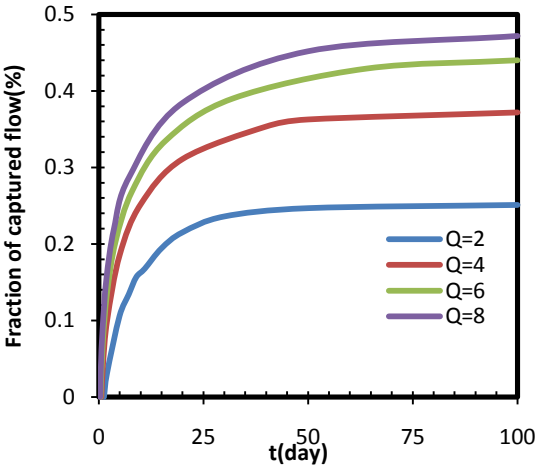

Figure 3.5. Particle arrival time distribution at the extraction chamber for a range of flow rate from 2 to 8 m^3/d for the structured K field.

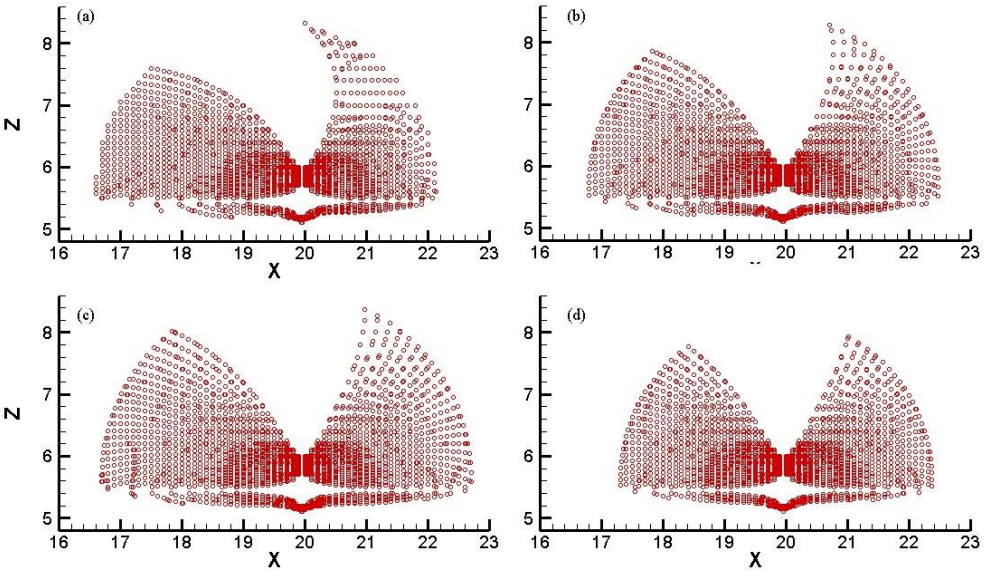

Figure 3.6. Dipole path lines when about 19% of flow returns for the structured K field at an injection rate of (a) 2, (b) 4, (c) 6 and (d) 8 m^3/d.

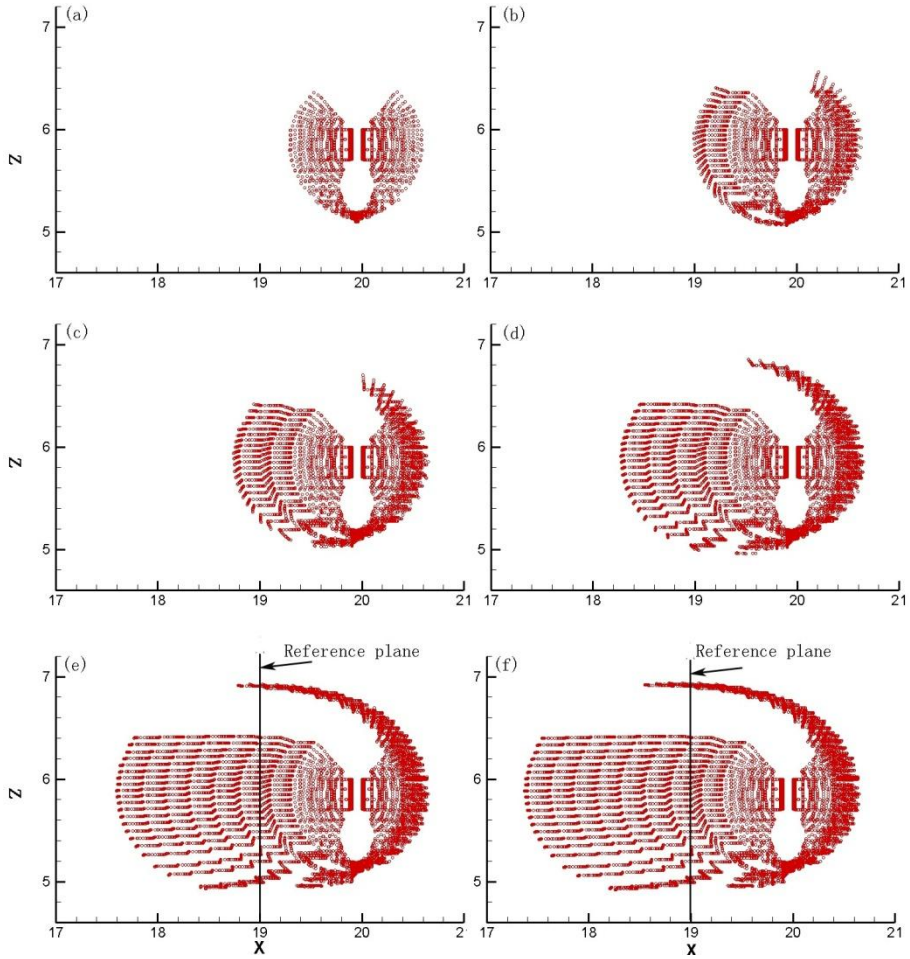

Figure 3.7. Forward tracking path lines originating from the dipole well in the homogeneous aquifer at the end of (a) the first injection cycle, (b) the second injection cycle, (c) the third injection cycle, (d) the fifth injection cycle, (e) the eighth injection and (f) at the ninth injection.

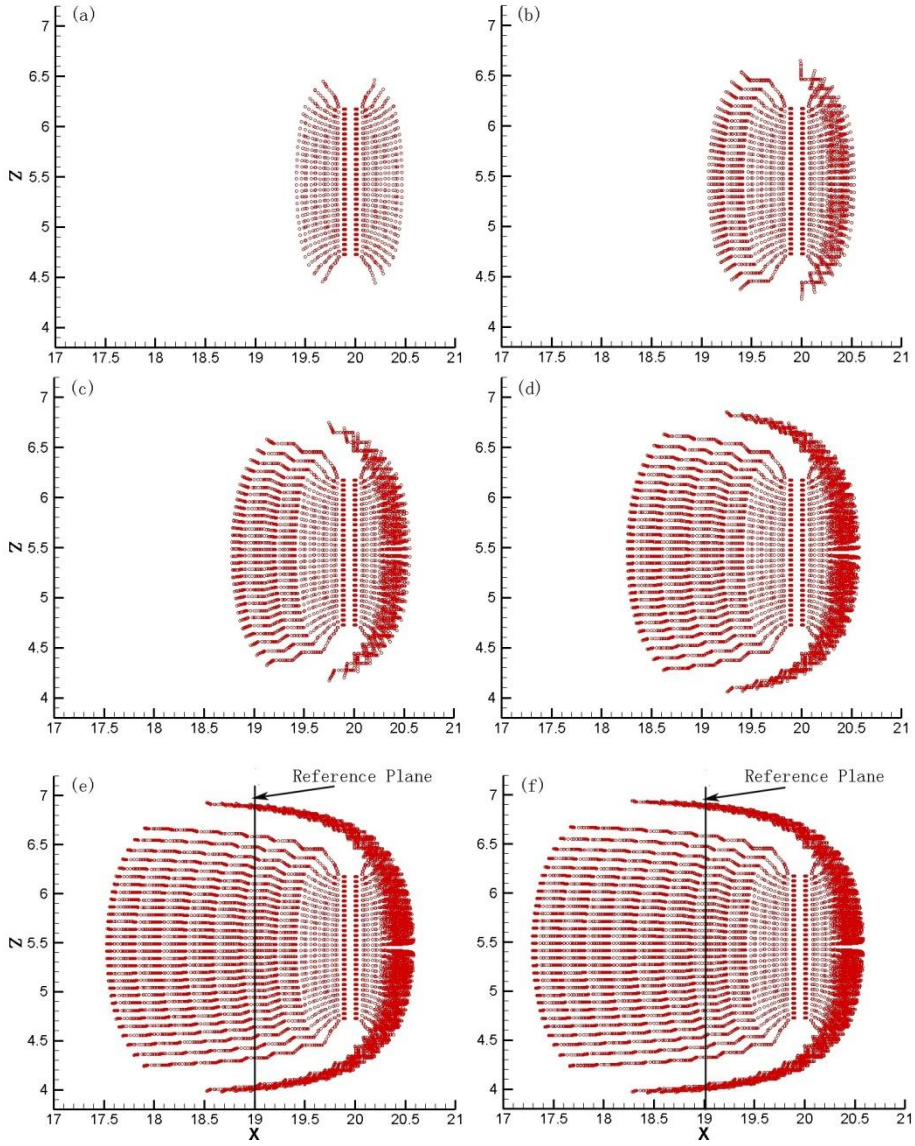

Figure 3.8. Forward tracking path lines originating from the single well in the homogeneous aquifer at the end of (a) the first injection cycle, (b) the second injection cycle, (c) the third injection cycle, (d) the fifth injection cycle, (e) the eighth injection cycle and (f) the ninth injection cycle.

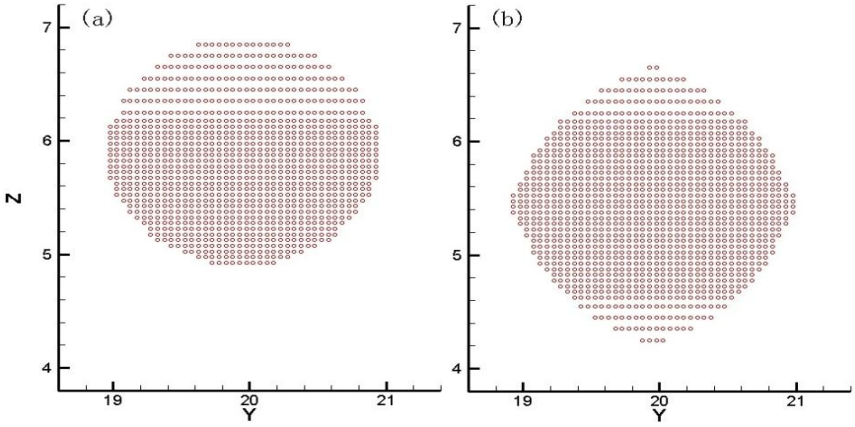

Figure 3.9. The shape of downstream coverage areas in the homogeneous aquifer for (a) dipole well and (b) single well.

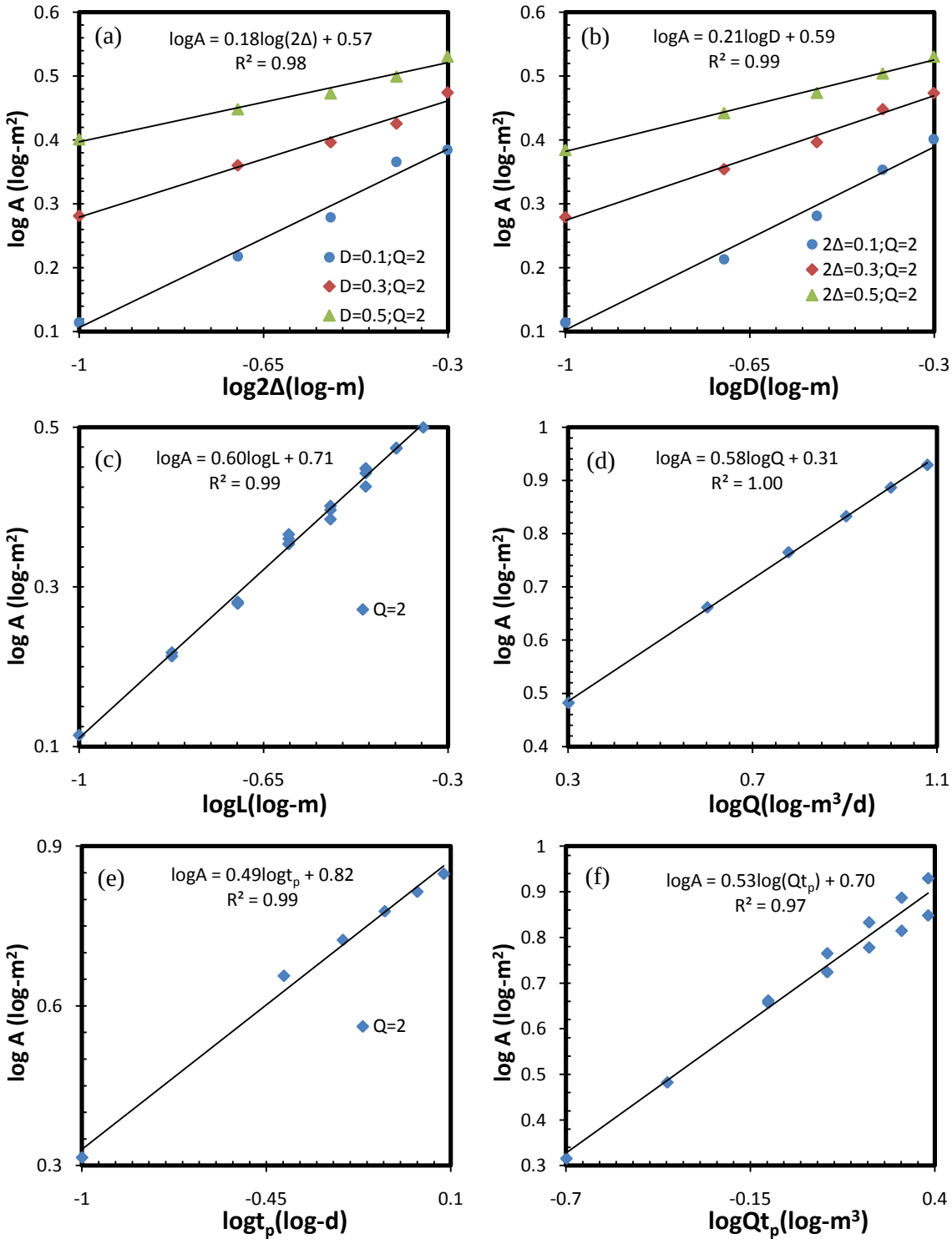

Figure 3.10. Plot of coverage area vs. system parameters: (a) chamber length (2Δ), (b) packer length (D), (c) shoulder length (L), (d) injection rate (Q), (e) pulsed injection time(t_p), (f) injection cost Qt_p.

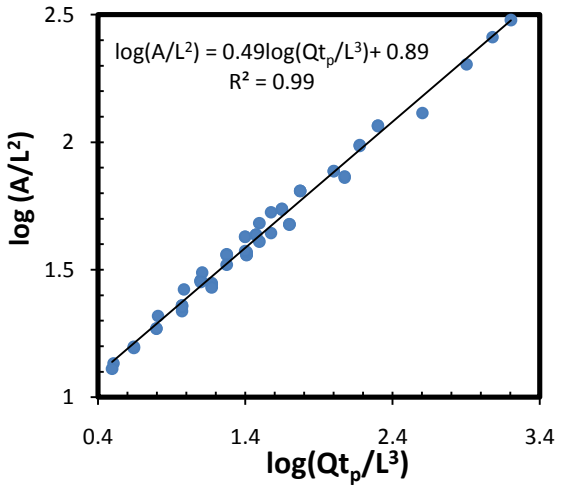

Figure 3.11. Normalized plot of dipole delivery performance.

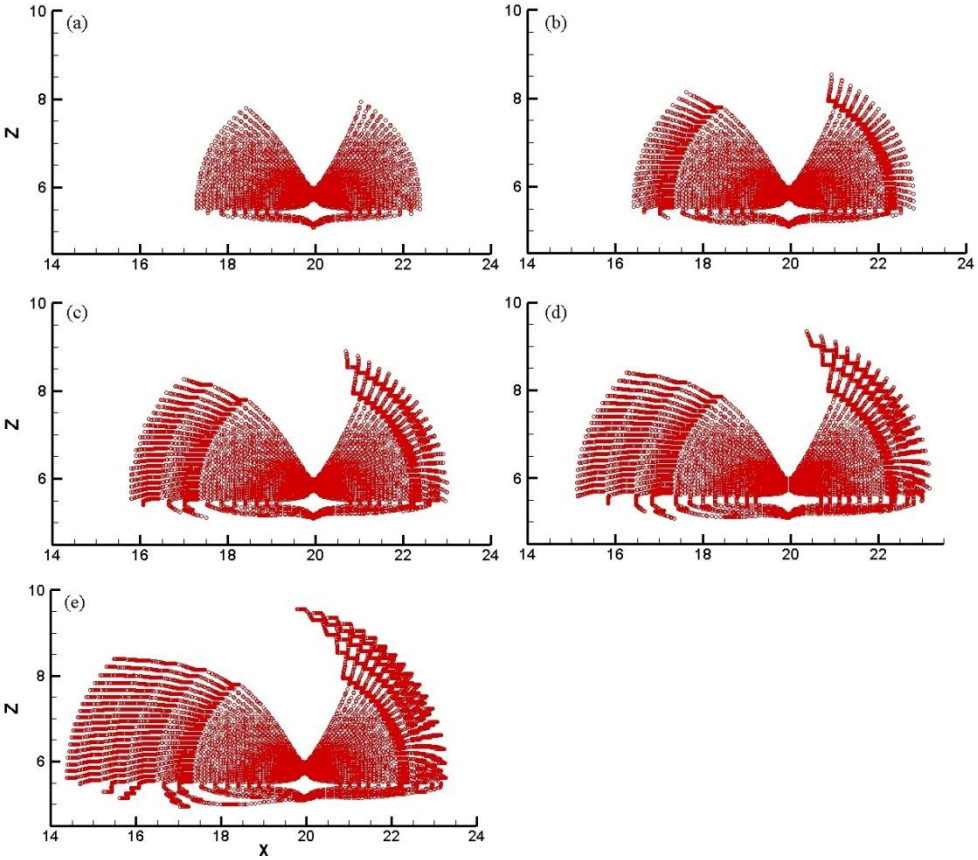

Figure 3.12. Dipole path lines in the structured K field with a 0.1 m thick layer of lower K in the middle of the domain at the end of: (a) the first injection cycle, (b) the second injection cycle, (c) the third injection cycle, (d) the fourth injection cycle and (e) the fifth injection cycle.

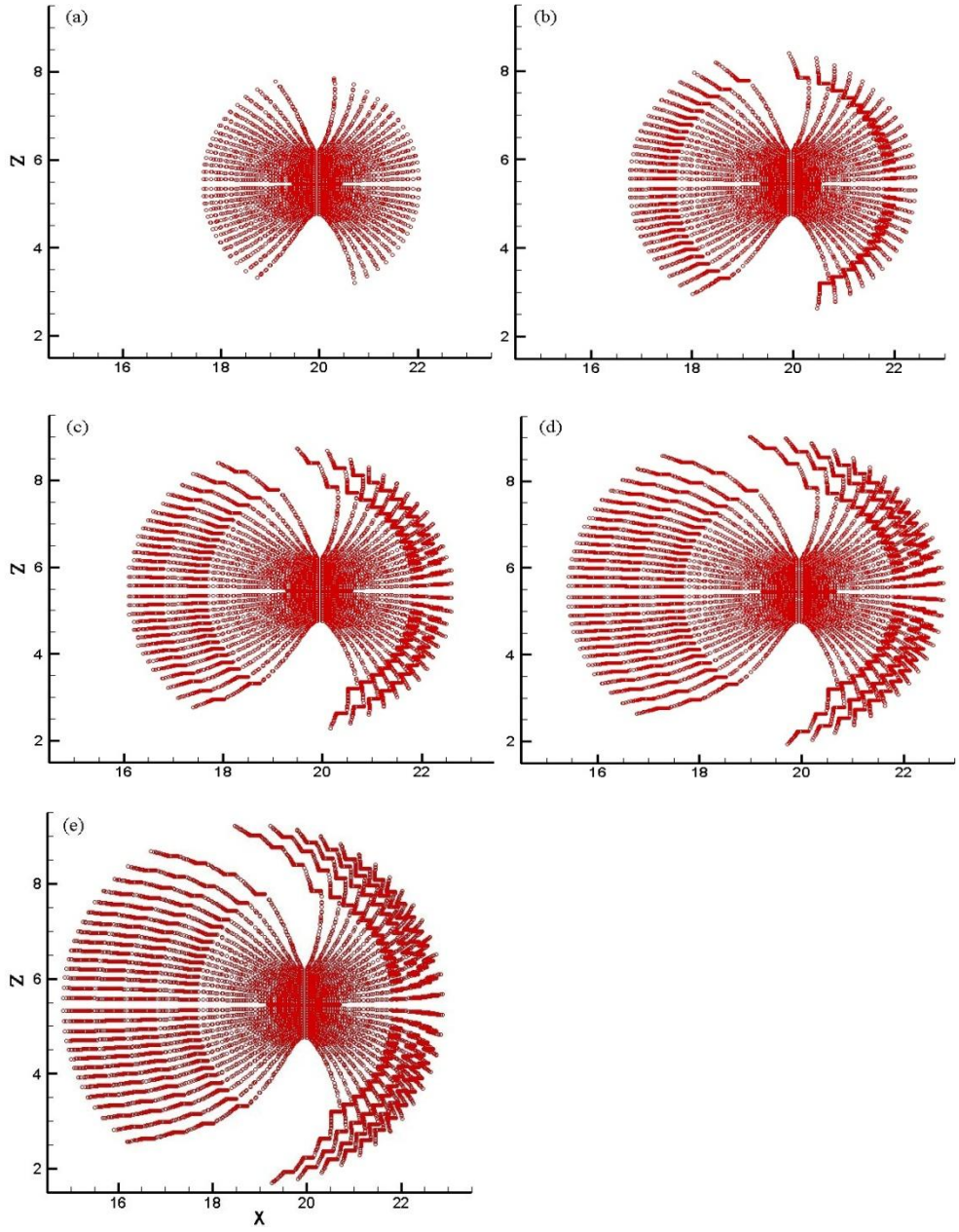

Figure 3.13. Single well path lines in the structured field with a 0.1 m thick layer of lower K in the middle of the domain at the end of the: (a) the first injection cycle, (b) the second injection cycle, (c) the third injection cycle, (d) the fourth injection cycle and (e) the fifth injection cycle.

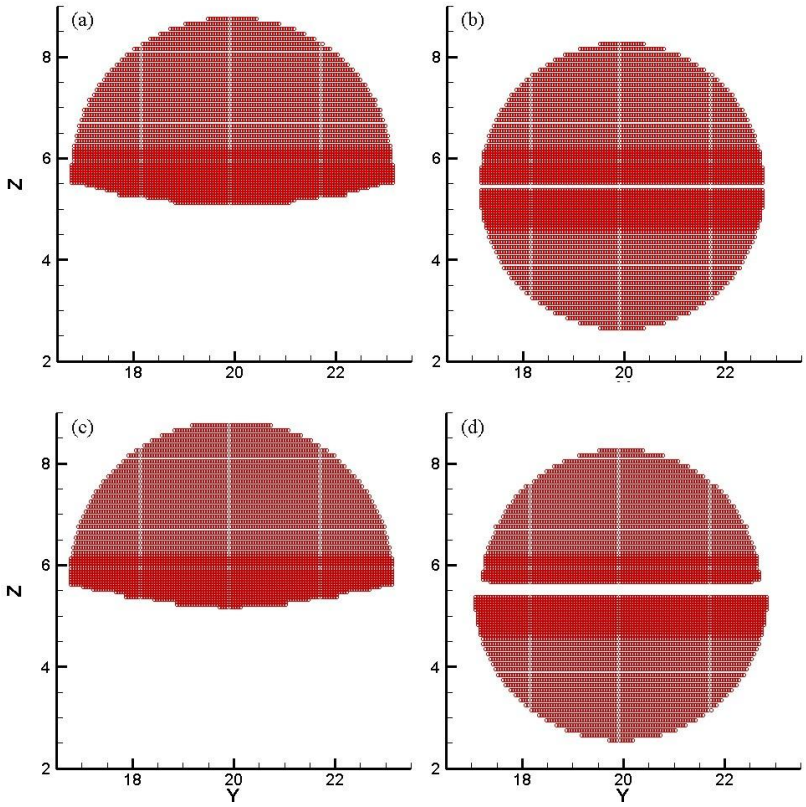

Figure 3.14. Downstream coverage area of: (a) dipole in the structured field with a 0.1 m thick layer of lower K in the middle of the domain, (b) single well in the structured field with a 0.1 m thick layer of lower K in the middle of the domain, (c) dipole in the structured field with a 0.2 m thick layer of lower K in the middle of the domain and (d) single well in the structured field with a 0.2 m thick layer of lower K in the middle of the domain.

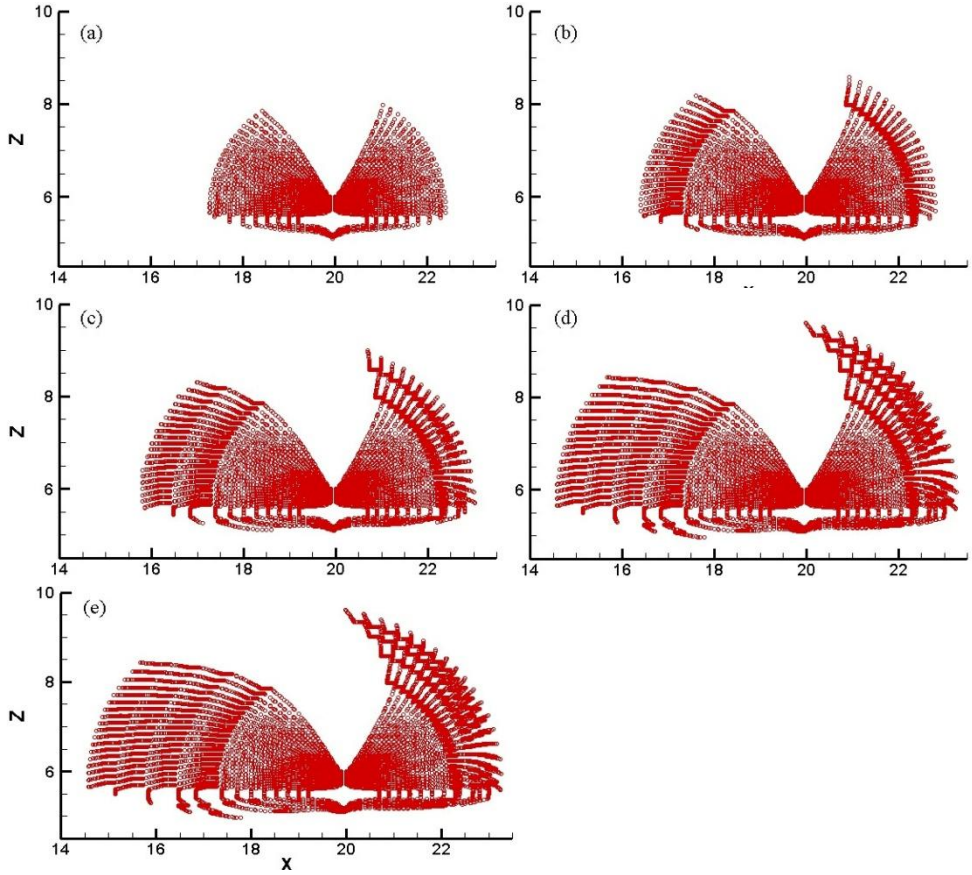

Figure 3.15. Dipole Path lines in the structured field with a 0.2 m thick layer of lower K in the middle of the domain at the end of: (a) the first injection cycle, (b) the second injection cycle, (c) the third injection cycle, (d) the fourth injection cycle and (e) the fifth injection cycle.

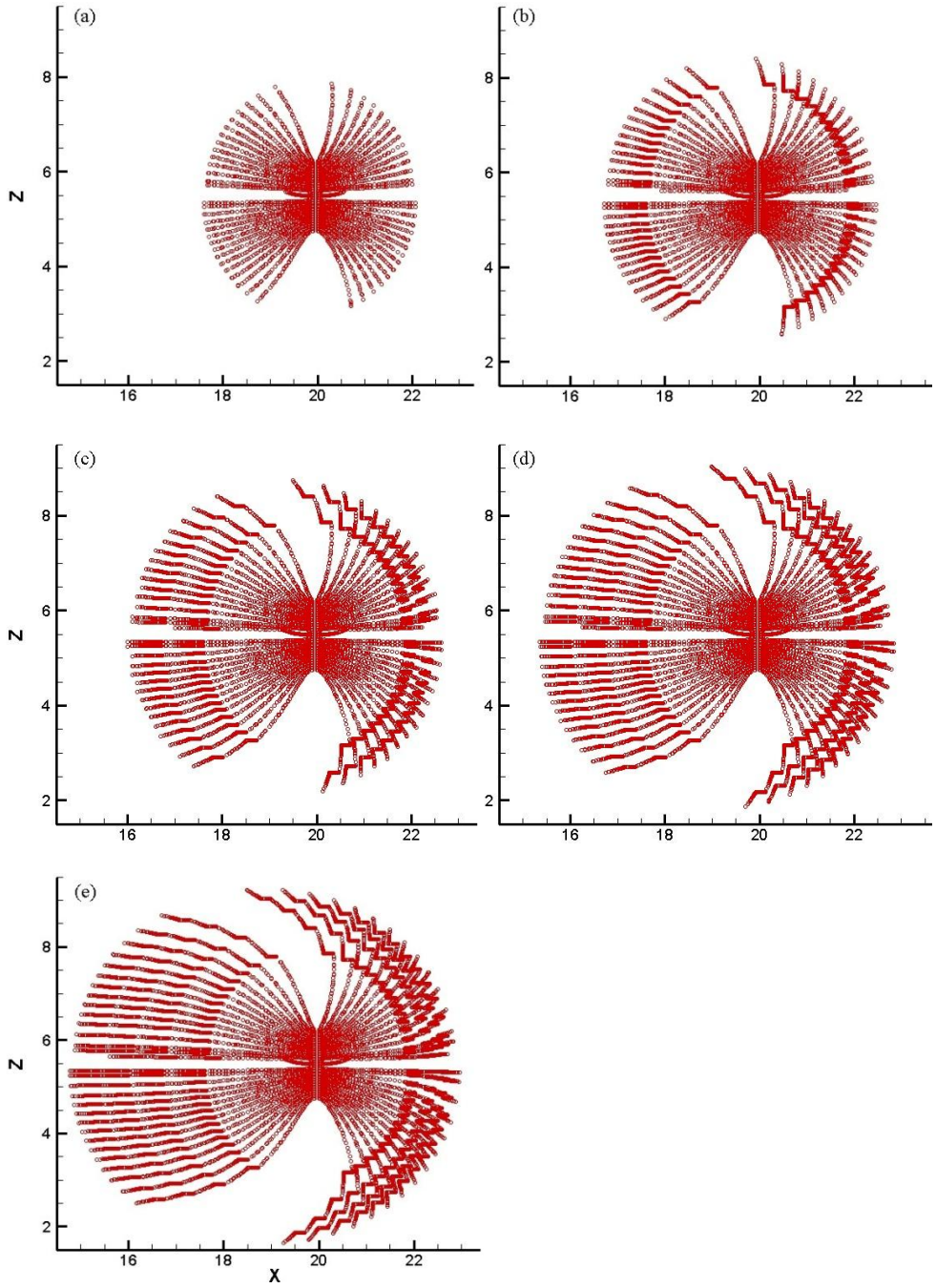

Figure 3.16. Single well path lines in the structured field with a 0.2 m thick layer of lower K in the middle of the domain at the end of: (a) the first injection cycle, (b) the second injection cycle, (c) the third injection cycle, (d) the fourth injection cycle and (e) the fifth injection cycle.

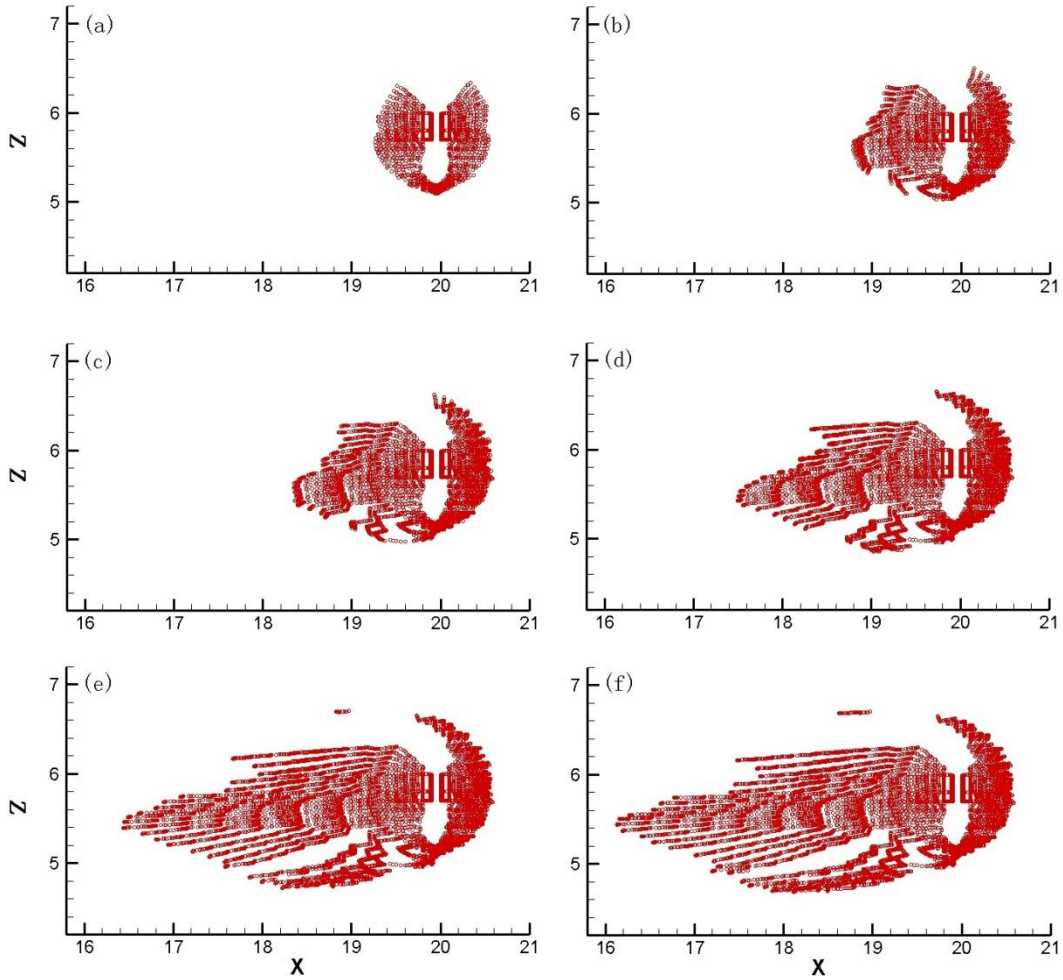

Figure 3.17. Dipole well path lines along the well in the Heterogeneous Field #1 at the end of (a) the first injection cycle, (b) the second injection cycle, (c) the third injection cycle; (d) the fourth injection cycle, (e) the eighth injection cycle and (f) ninth injection cycle.

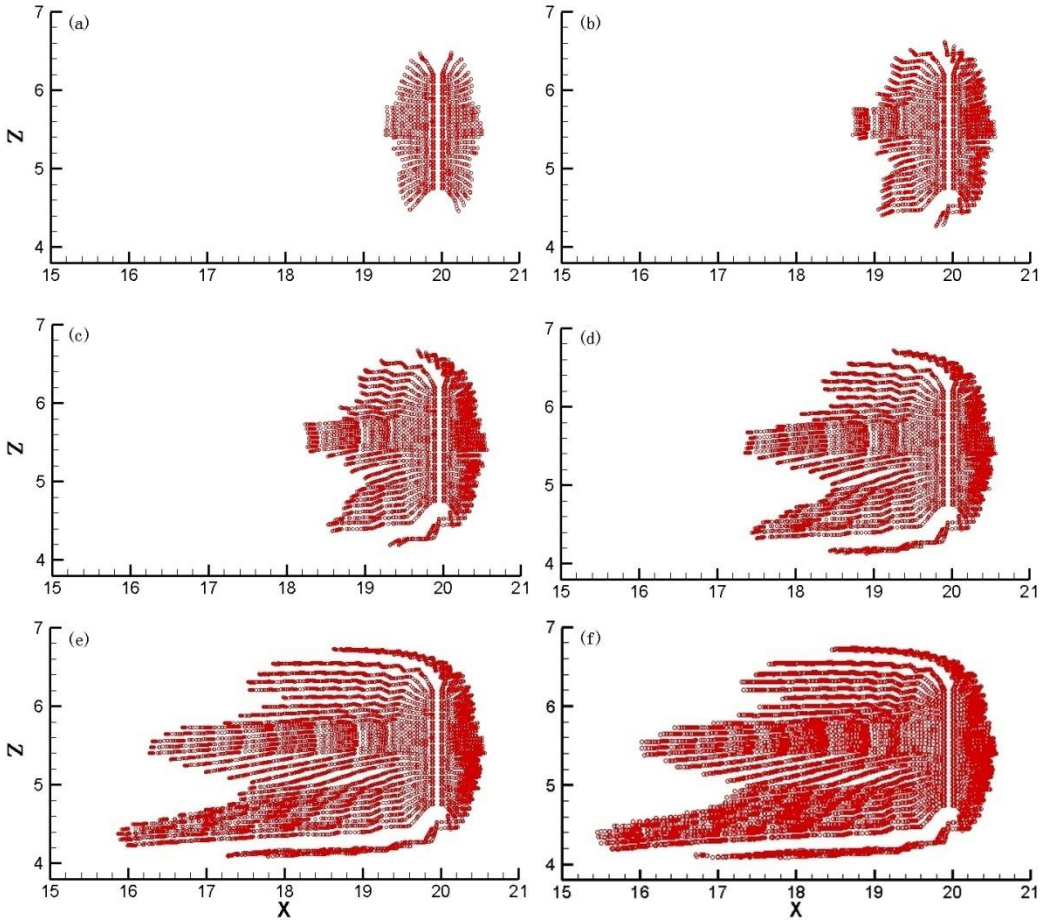

Figure 3.18.Single well flow lines along the well in Heterogeneous Field #1 at the end of (a) the first injection cycle, (b) the second injection cycle, (c) the third injection cycle; (d) the fourth injection cycle, (e) the eighth injection cycle and (f) ninth injection cycle.

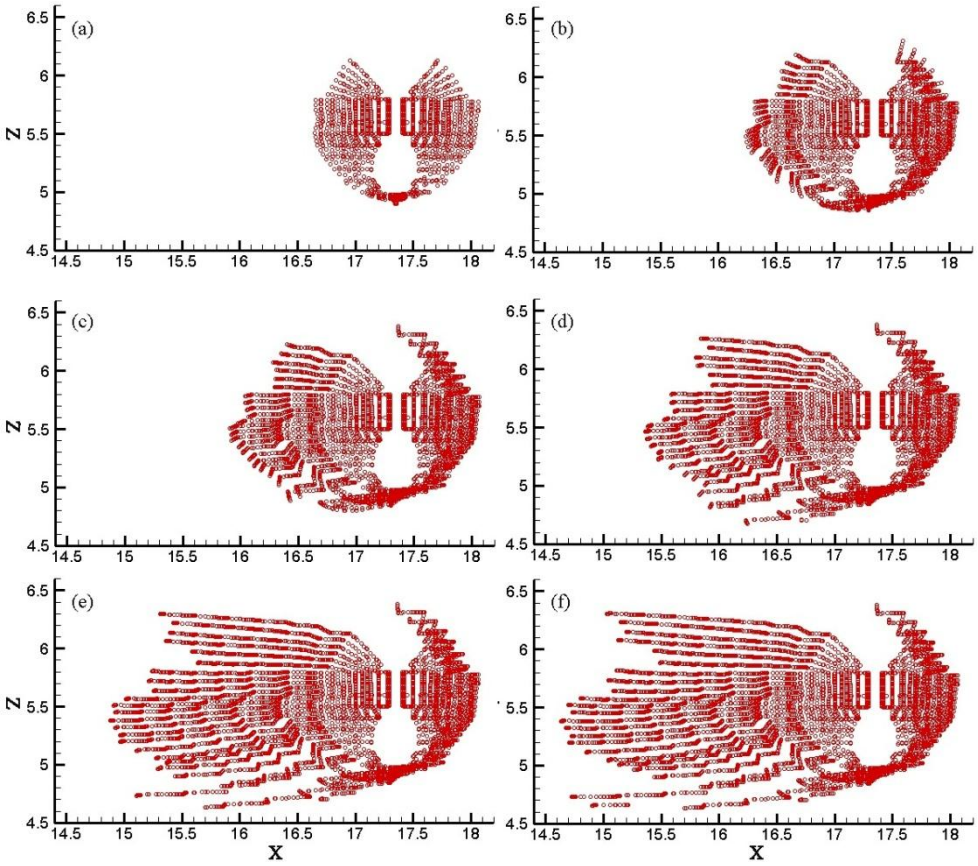

Figure 3.19.Dipole flow lines along the well at Location A in Heterogeneous Field #1 at the end of (a) first injection cycle, (b) the second injection cycle, (c) the third injection cycle, (d) the fifth injection cycle, (e) the eighth injection cycle and (f) the ninth injection cycle.

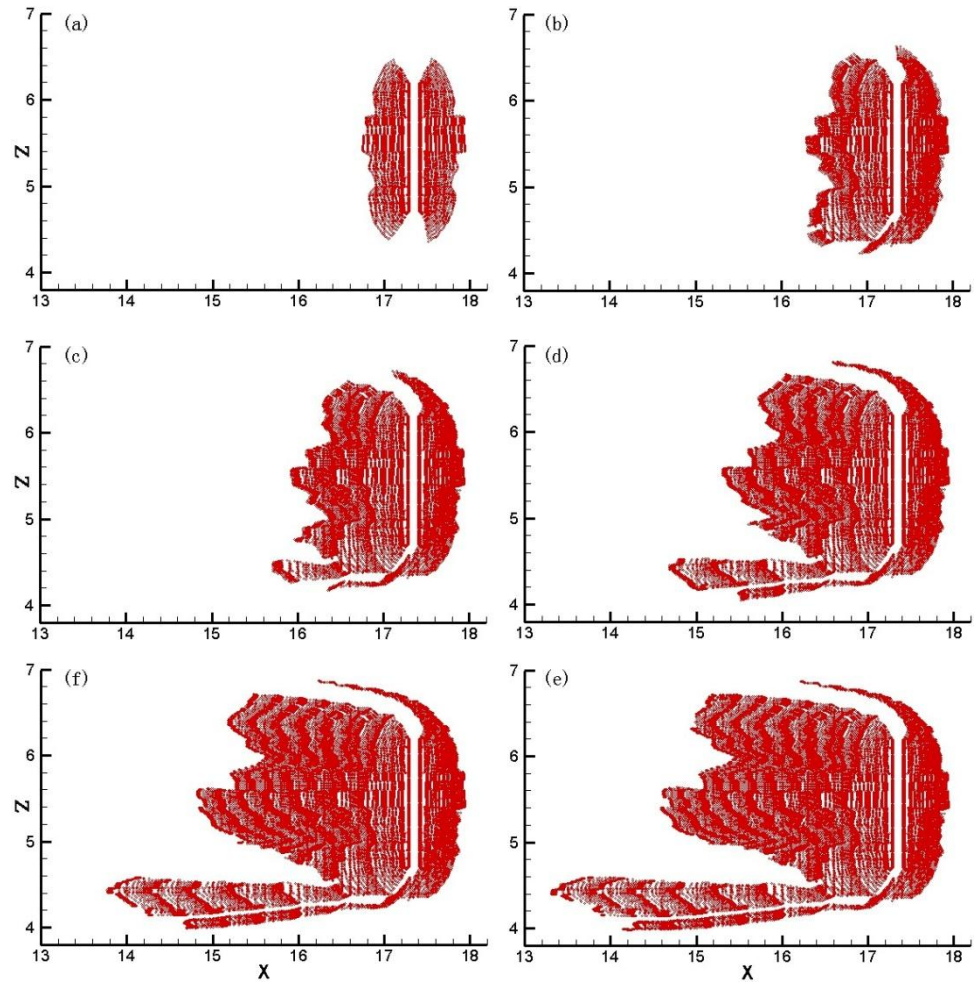

Figure 3.20. Single well flow lines along the well at Location A in Heterogeneous Field #1 at the end of (a) first injection cycle, (b) the second injection cycle, (c) the third injection cycle, (d) the fifth injection cycle, (e) the eighth injection cycle and (f) the ninth injection cycle.

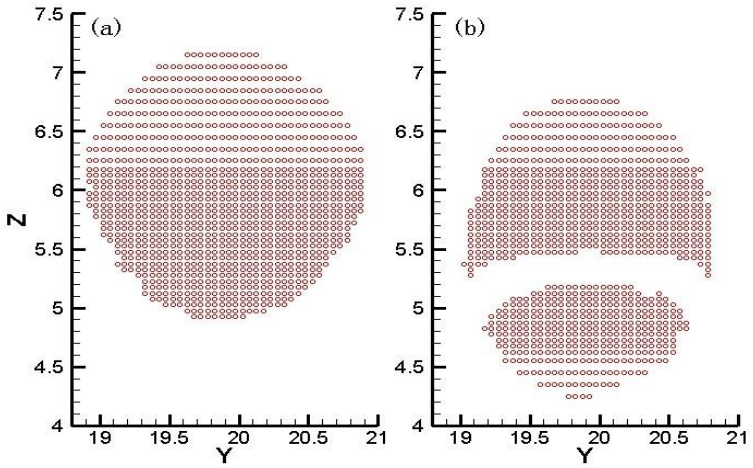

Figure 3.21. Downstream coverage area at Location A in Heterogeneous Field #1 for (a) dipole well and (b) single well.

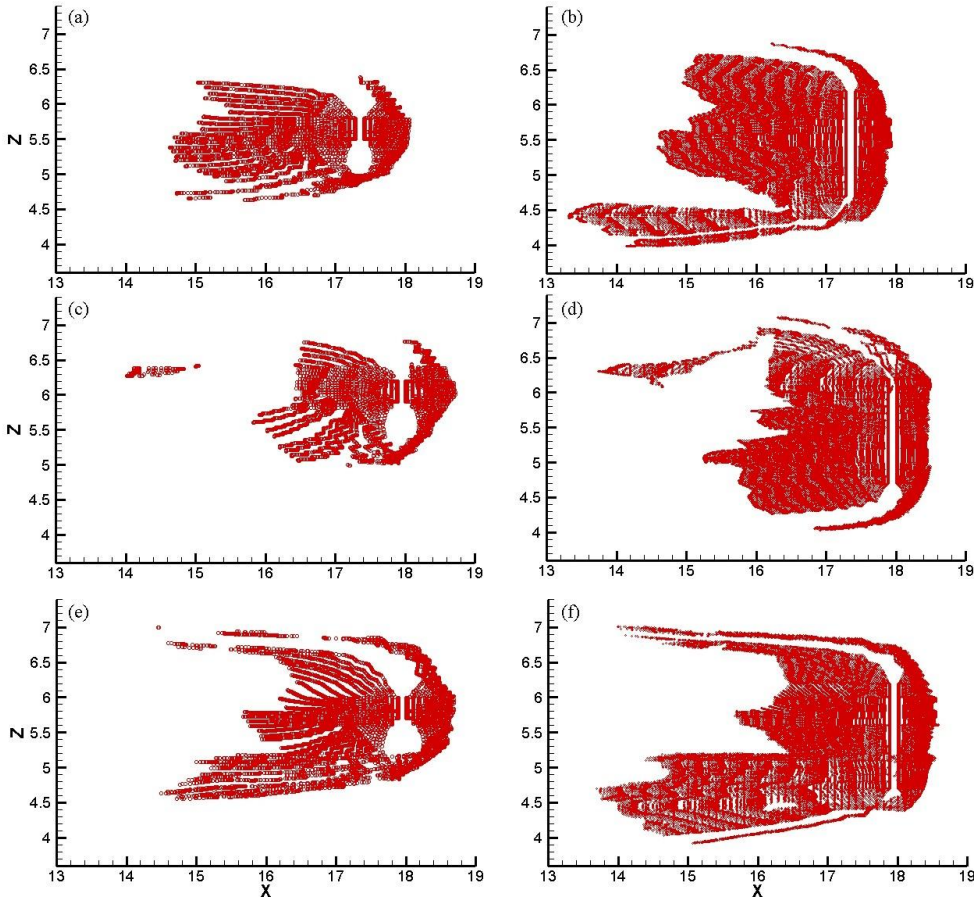

Figure 3.22. Path lines originating from the well at the end of the eighth injection cycle for: (a) dipole well in Heterogeneous Field #1, (b) single well in Heterogeneous Field #1, (c) dipole well in Heterogeneous Field #2, (d) single well in Heterogeneous Field #2, (e) dipole well in Heterogeneous Field #3 and (f) single well in Heterogeneous Field #3.

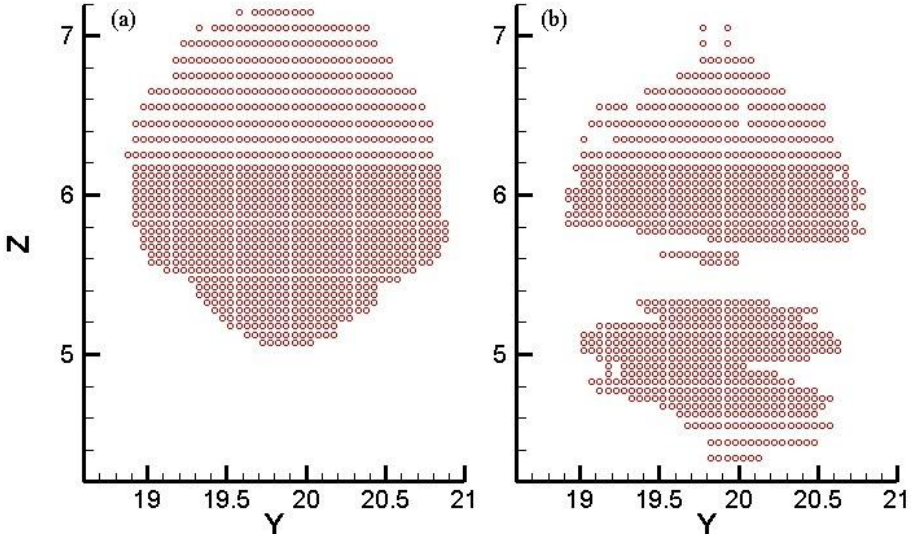

Figure 3.23. The shape of downstream coverage area in Heterogeneous Field #2 for (a) dipole well and (b) single well.

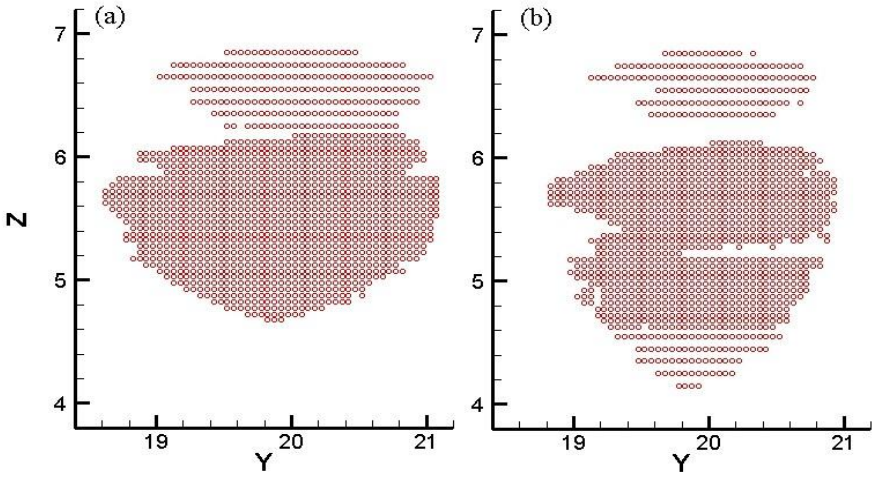

Figure 3.24. The shape of downstream coverage area in Heterogeneous Field #3 for (a) dipole well and (b) single well.

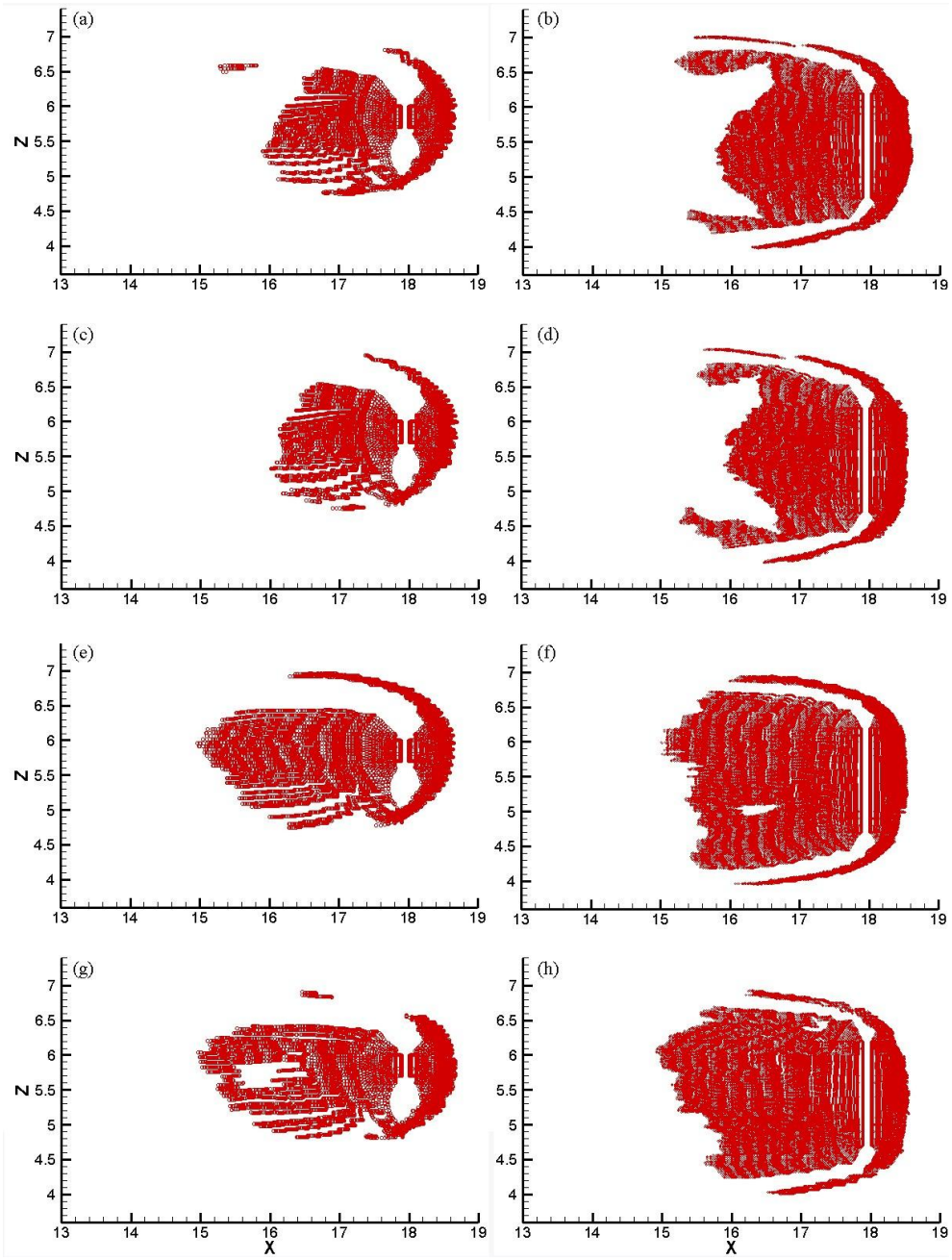

Figure 3.25. Path lines originating from the well at the end of the eighth injection cycle for: (a) dipole well in Heterogeneous Field #4, (b) single well in Heterogeneous Field #4, (c) dipole well in Heterogeneous Field #5, (d) single well in Heterogeneous Field #5, (e) dipole well in Heterogeneous Field #6, (f) single well in Heterogeneous Field #6, (g) dipole well in Heterogeneous Field #7 and (h) single well in Heterogeneous Field #7.

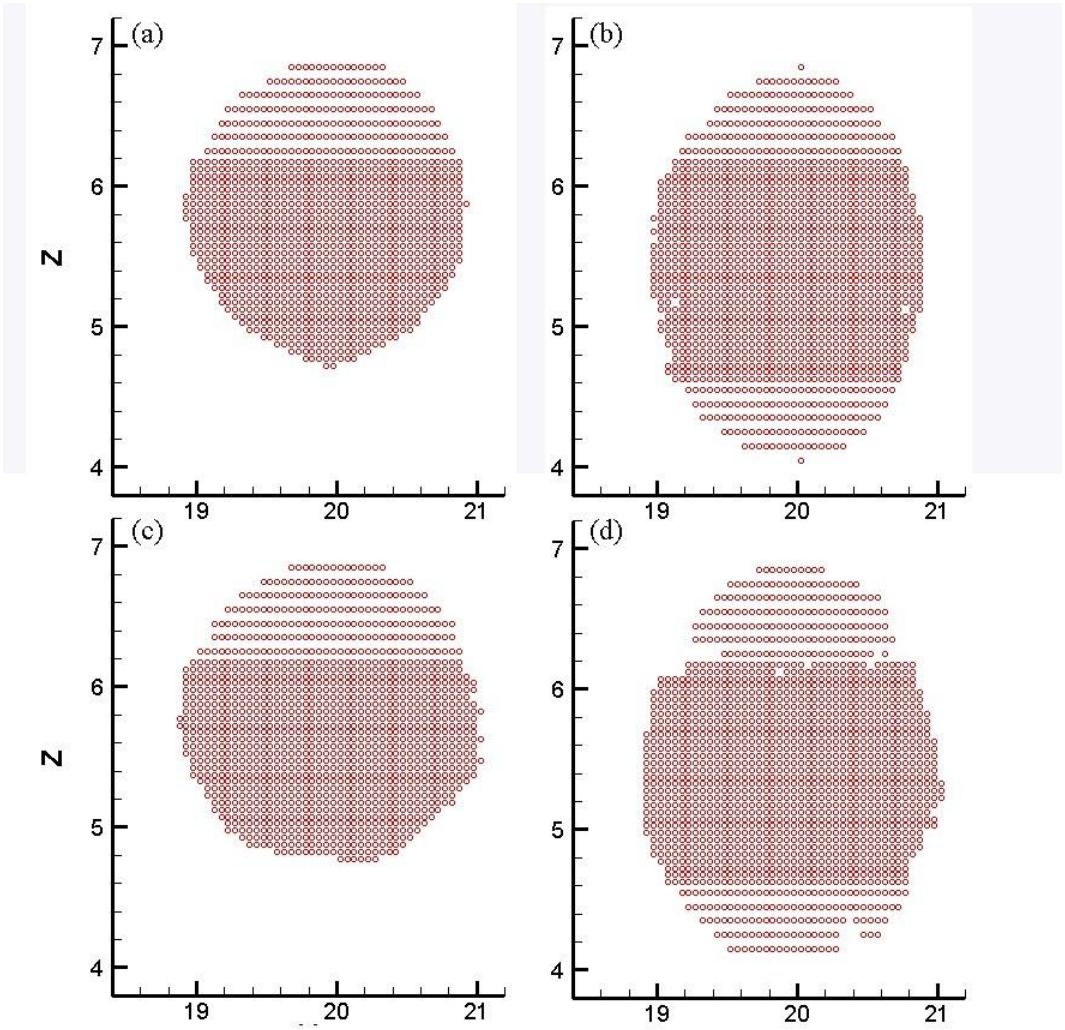

Figure 3.26. The shape of the downstream coverage area for (a) dipole well in Heterogeneous Field #6, (b) single well in Heterogeneous Field #6, (c) dipole well in Heterogeneous Field #7 and (d) single well in Heterogeneous Field #7.

Table 3.1 Grid size and domain discretization.

	Range(m)	size(m)	number of cells
x axis	0~8; 32~40	2.0	8
	8~10; 30~32	1.0	4
	10~12; 28~30	0.5	8
	12~14; 26~28	0.25	16
	14~15; 25~26	0.2	10
	15~25	0.1	100
y axis	0~8; 32~40	2.0	8
	8~10; 30~32	1.0	4
	10~12; 28~30	0.5	8
	12~14; 26~28	0.25	16
	14 ~15;25~26	0.2	10
	15~25	0.1	100
z axis	0~1; 10~11	0.5	4
	1~2; 9~10	0.25	8
	2~4.6; 6.2~9	0.2	27
	4.6~6.2	0.1	16

Table 3.2 Statistical properties of the random permeability fields used in heterogeneous simulations

Field	Variance [log-m^2/d^2]	Correlation-xy [m]	Correlation-z [m]
1	0.29	2.8	0.12
2	0.50	2.8	0.12
3	1.00	2.8	0.12
4	0.29	1.4	0.12
5	0.29	0.7	0.12
6	0.29	0.1	0.12
7	0.50	0.1	0.12

Chapter Four Conclusions and Recommendations

4.1 Conclusions

In this research, mathematical tools were used to simulate the relative efficacy of dipole and single wells for delivering reagent to a subsurface contaminant plume. For the investigation of steady-state delivery performance, a simple analytical model was adopted. For transient study, MODFLOW-2000 and MODPATH were used to simulate the flow field and particle paths respectively. Instead of calculating the complicated volume of the coverage zones swept by the injection wells, either coverage area around the well or down gradient coverage area was used as a basis for comparison. A sensitivity analysis was conducted to assess the impact of dipole configuration, injection cost, and the hydraulic conductivity distribution on coverage area.

The simulation results show that the dipole well configuration can influence reagent delivery behaviour. The impact of the shoulder length on delivery performance is consistent in both steady-state and transient investigations; an increased shoulder length (2L) will improve performance. An increase in the injection cost (assumed to be directly proportional to the volume of injected fluid per pulse, Qt_p) will also increase the coverage area. Based on the results from the transient investigation, the half shoulder length (L) and the injection cost are the characteristic parameters that control dipole well performance. An empirical relationship between coverage area and the system characteristic parameters was identified which can be used as a design tool of low injection volumes (i.e., $\leq$ 0.4 m^3) in a relatively homogeneous aquifers.

With an appropriate injection schedule, the dipole well can deliver a reagent solution into the lower hydraulic conductivity zone but single well cannot. In the heterogeneous hydraulic conductivity fields, the location of the lower hydraulic conductivity lenses relative to the injection wells is important. As expected, the dipole well forces the injected reagent through the low permeable zones and thus outperforms single well in some of the heterogeneous aquifers investigated. The findings also show that as the degree of heterogeneity increases, the dipole well performance decreases correspondingly and the advantage of dipole delivery over the single well delivery is less. Moreover, when the horizontal extent of bedding planes is small (e.g., 0.1 m $\times$ 0.1 m $\times$ 0.12 m along x, y and z-axis), the single well can perform as well as dipole well system and thus is a preferred delivery method considering its simple configuration.

4.2 Recommendations

This research performed in this thesis used mathematical tools to investigate the delivery performance of dipole well system. This investigation was confined to a well complete with a standard screen length of 1.5 m under the purely advective flow. It is, of course, difficult to generalize these results to more general aquifer systems. Therefore, future investigations should be extended to:

- Perform a more extensive sensitivity analysis in order to more completely characterise the effectiveness of the dipole delivery system over a wider range of system configurations and aquifer parameters;
- Simulate the dipole well behaviour (the same system configuration as in this research) in randomly heterogeneous hydraulic conductivity fields with the presence of stagnant or

dual porosity zones and assess the impact of the stagnant zones on the reagent distribution;

- Conduct dipole conservative tracer test at multiple locations in Borden Aquifer to measure the distribution of the injected tracer and thus confirm the findings from the research;
- Investigate the effect of dispersion, sorption and chemical reaction on the distribution of selected reagents delivered by dipole well and single well;
- Evaluate dipole well delivery efficiency by assessing the contaminant mass destructed by the injected reagent relative to a single well delivery system; and
- Design and apply the delivery system of dipole wells (i.e., spacing and depth of the dipole wells, and the injection schedule) on specific contaminated sites.

References

Bagagaoglu, H. G. (2002). Transport in heterogeneous media: tracer dynamics in complex flow networks. *Environmental and Energy Engineering, 48(5):* 1121-1131.

Boulding, J. R. (1996). Environmental engineering source book. Michgan: Ann Arbor Press Inc. pp. 31-32;171.

Craig, J. R. (2004). *Reactive Contaminant Transport Modeling Using Analytic Element Flow Solutions.* PhD Thesis,Department of Civil, Structural, and Environmental Engineering,The State University of New York at Buffalo, Bufflo, NY.

Craig, J.R.(2009). *Dipole3D software design notes, unpublished technical report.* Department of Civil & Environmental Engineering, University of Waterloo, Waterloo, ON.

Cunningham, J. A., Hoelen, T. P., Hopkins, G. D., Lebron, C. A., & Reinhard, M. (2004). Hydraulics of recirculating well pairs for groundwater remediation. *Groundwater,42(6):* 880-889.

Frind, E. O., Molson, J. W., & Schirmer, M. Dissolution and mass transfer of multiple chlorinated hydrocarbons under field conditions. *Groundwater Quality: Remediation and Protection 98 Conference,* Tubingen, Germany, 1998.

Harbaugh, A. W., Banta, E. R., Hill, M. C., & McDonald, M. G. (2000). *MODFLOW-2000, THE U.S. Geological Survey Modular Groundwater Model—User Guide To Modularization Concepts and The Groundwater Flow Process.* U.S. Geological Survey Open-File Report 00-92.

Hassinger, E., & Watson, J. (1995). Health effects of drinking water. *EPA protocol for the review of existing national primary drinking water regulations (EPA 815-R-03-002).*

Kabala, A. (1993). The dipole flow test: a new single-borehole test for aquifer characterization. *Water Resources Research, 29(1):* 99-107.

Krešić, N. (2007). Hydrogeology and groundwater modeling. FL: CRC Press. pp. 466.

MacFarlane, D., Cherry, J., Gillham, R., & Sudicky, E. (1983). Migration of contaminants in groundwater at a landfill: a case study. *Journal of Hydraology,* 63: 1-29.

Mackay, D., & J.A.Cherry. (1989). Groundwater contamination: Pump-and-treat remediation. *Environmental Science and Technology* , 23(6): 168-170.

Martin, T. A., & Ruby, M. V. (2004). Review of in-situ remediation technologies for lead, zinc, and cadminum in soil. *Remediation Journal, 14(3):* 35-53.

Muskat, M. (1937). *The flow of homogeneous fluids through porous media.* New York: McGraw-Hill.

Nyer, E. K., Carman, E. P., Boettcher, G., Bedessem, J. M., Lenzo, F., Crossman, T. L., et al. (2001). In *In-situ treatment technology*. CRC Press LLC. pp. 3-13

Patrick, R., Ford, E., & Quarles, J. (1987). Groundwater contamination in the United States. Pheladelphia: University of Pennsylvania Press. pp. 4-5.

Peursema, D., Zlotnik, V., & Ledder, G. (1999). Groundwater flow near vertical recirculatory wells: effect of skin on flow geometry and travel times with implications for aquifer remediation. *Journal of Hydraology (222)*: 109-122.

Pollock, D. (1994). *User's Guide for MODPATH/MODPATH-Plot, Version 3: A particle tracking post-processing package for MODFLOW, the U.S. Geological Survey finite-difference ground-water flow model.* U.S. Geological Survey Open-File Report 94-464.

Prakash, A. (2004). Water Resource Engineering: handbook of essential methods and design. Reston, Virginia: American Society of Civill Engineers: 150.

Rail, D.Chester. (2000). Groundwater Contamination, Volume II: Management, Containment, Risk Assessment and Legal Issues. CRC Press.

Reiha, B. (2006). *A numerical interpretation model for the dipole flow and reactive tracer test.M.A.Sc. Thesi,* Department of Civil and Environmental Engineering, University of Waterloo, Waterloo, ON.

Robin, M. J., Gutjahr, A., Sudicky, E., & Willson, J. (1993). Cross-correlated random field generation with the Direct Fourier Transform method. *Water Resources Research, 29(7):* 2385-2397.

Roos, G. (2008). *Development of the dipole flow and reactive tracer test(DFRTT) for aquifer parameter estimation.* M.A.Sc Thesis, Department of Civil and Environmental Engineering, University of Waterloo, Waterloo, ON.

Sawyer, C. S., & Lieuallen, D. (1998). Productivity comparison of horizontal and vertical groundwater remediation well scenarios. *Groundwater, 36(1)*: 98-103.

Seol, Y., Zhang, H., & Schwartz, F. (2003). A Review of In-situ Chemical Oxidation and Heterogeneity. *Environmental and Engineering Geoscience, 9(1):* 37-49.

Starr, R. C., & Cherry, J. A. (1994). In-situ remediation of contaminated groundwater: the funnel-and-gate system. *Groundwater,32(3)*: 465-476.

Steward, D. R., & Jin, W. (2003). Drawdown and capture zone topology for nonvertical wells. *Water Resources Research, 39(8):* 1219-1229.

Strack, O.D.L. (1989). *Groundwater Mechanics.* Prentice-Hall, Old Tappan, N.J.

Sturnman, P., Stewart, P., Cunningham, A., Bouwer, E., & Walfram, J. (1995). Engineering scale-up of in-situ bioremediation process: A review. *Journal of Contaminant Hydrology,19:* 171-203.

Sudicky, E.A. (1986). A Natural Gradient Experiment on Solute Transport in a Sand Aquifer:Spatial Variability of Hydraulic Conductivity and Its Role in the Dispersion Process. *Water Resources Research*, 22(1): 2069-2082.

Sutton, D., Kabala, Z., Schaad, D., & Ruud, N. (1999). The dipole-flow test with a tracer: a new single-borehole tracer test for aquifer characterization. *Journal of Contaminant Hydraology (44)*: 71-101.

Thomson, N., Reiha, B., McKnight, D., Smalley, A., & Banwart, S. (June 2-4, 2005). An overview of the dipole flow in sity reactor. *In Proceedings,33rd Annual Conference of the Canadian Society for Civil Engineering.* Toronto.

USEPA. (1998). *Permeable reactive barrier technologies for contaminant remediation.* (EPA 600-R-98-125).

USEPA. (2003). The DNAPL remediation challenge: is there a case for source depletion? *(EPA 600-R-03-143)* .

USGS. (1996). *Sources and Extent of Groundwater Contamination.* (US geological survey,AG-441-4).

Zlotnik, V., & Zurbuchen, B. (1998). Dipole probe: design and field applications of a single borehole device for measurements of vertical variations of hydraulic conductivity. *Groundwater, 36(6)*: 884-893.

Zlotnik, V., & Zurbuchen, B. (2003). Field study of hydraulic conductivity in a heterogeneous aquifer: Comparison of single-borehole measurements using different instruments. *Water Resources Research,39(4):* 1101.

Zlotnik, V., Zurbuchen, B., & Ptak, T. (2001). The steady state dipole flow test for characterization of hydraulic conductivity statistics in a highly permeable aquifer:Horkheimer Insel site, Germany. *Groundwater,39(4):* 504-516.

Appendix A

Taking $\xi = x - \tilde{x}$, Eq. (2.2) is rewritten as:

$$\Phi = -\frac{1}{4\pi}\int_{x-L}^{x+L} \frac{\sigma_0 + \frac{\sigma_1}{L}(x-\xi)}{(\xi^2 + y^2 + z^2)^{1/2}} d\xi \qquad \text{A (1)}$$

Using Eq. A(2) and A(3) (equation 233.15a of Gröbner and Hofreiter [1975]):

$$\int \frac{1}{(x^2 + \alpha^2 + \beta^2)^{1/2}} dx = \ln\left[(x^2 + \alpha^2 + \beta^2)^{\frac{1}{2}} + x\right] \qquad \text{A (2)}$$

and

$$\int \frac{x}{(x^2 + \alpha^2 + \beta^2)^{1/2}} = (x^2 + \alpha^2 + \beta^2)^{1/2} \qquad \text{A (3)}$$

Eq. A(1) can be solved:

$$\Phi = -\frac{\sigma_0 + \frac{\sigma_1}{L}\tilde{x}}{4\pi} \ln\frac{\tilde{r}^+ - \tilde{x}^+}{\tilde{r}^- + \tilde{x}^-} + \frac{\sigma_1}{L}\frac{1}{4\pi}(\tilde{r}^+ - \tilde{r}^-) \qquad \text{A (4)}$$

$$\tilde{r}^+ = \sqrt{(\tilde{x} + L)^2 + \tilde{y}^2 + \tilde{z}^2} \qquad \text{A (5)}$$

$$\tilde{x}^+ = (\tilde{x} + L) \qquad \text{A (6)}$$

$$\tilde{r}^- = \sqrt{(\tilde{x} - L)^2 + \tilde{y}^2 + \tilde{z}^2} \qquad \text{A (7)}$$

$$\tilde{x}^- = (\tilde{x} - L) \qquad \text{A (8)}$$

where $\tilde{x}$, $\tilde{y}$, $\tilde{z}$ are the local coordinate system along x, y, z-axis, L is the half length of line segment [L], and σ_0, σ_1 are the strength coefficients [L^2/T].

Then flow rates along axes x, y, z can be obtained by differentiate the Eq. A(4) by x, y, z respectively:

$$q_x = \frac{(\sigma_0 - \sigma_1)}{4\pi}\frac{1}{\tilde{r}^+} - \frac{(\sigma_0 + \sigma_1)}{4\pi}\frac{1}{\tilde{r}^-} + \frac{\sigma_1}{L}\frac{1}{4\pi}\ln\frac{\tilde{r}^+ + \tilde{x}^+}{\tilde{r}^- + \tilde{x}^-} \qquad \text{A (9)}$$

$$q_y = -\frac{\sigma_0 + \frac{\sigma_1}{L}\tilde{x}}{4\pi}\frac{\tilde{y}}{\tilde{V}^2}\left(\frac{\tilde{x}^+}{\tilde{r}^+} - \frac{\tilde{x}^-}{\tilde{r}^-}\right) - \frac{\sigma_1}{L}\frac{\tilde{y}}{4\pi}\left(\frac{1}{\tilde{r}^+} - \frac{1}{\tilde{r}^-}\right) \qquad A\,(10)$$

$$q_z = -\frac{\sigma_0 + \frac{\sigma_1}{L}\tilde{x}}{4\pi}\frac{\tilde{z}}{\tilde{V}^2}\left(\frac{\tilde{x}^+}{\tilde{r}^+} - \frac{\tilde{x}^-}{\tilde{r}^-}\right) - \frac{\sigma_1}{L}\frac{\tilde{z}}{4\pi}\left(\frac{1}{\tilde{r}^+} - \frac{1}{\tilde{r}^-}\right) \qquad A\,(11)$$

$$\tilde{V} = \sqrt{\tilde{y}^2 + \tilde{z}^2} \qquad A\,(12)$$

Flow rate of line source in dipole should be the same with line sink but in the opposite direction. For each point sink or point source, the solutions (Eq. A(9),A(10),A(11)) are transformed to the ordinary coordinate system, and adding all the solutions together as well as regional groundwater flow, final solutions are obtained:

$$\begin{aligned}\Phi = &\sum_{i=1}^{n} -\frac{\sigma_0^i + \frac{\sigma_1^i}{L}\left[x + \frac{D}{2} + L(2i-1)\right]}{4\pi}\ln\frac{(r_{up}^+ + x_{up}^+)}{(r_{up}^- + x_{up}^-)} \\ &+ \sum_{i=1}^{n}\frac{\sigma_0^i + \frac{\sigma_1^i}{L}\left[x - \frac{D}{2} + L(2i-1)\right]}{4\pi}\ln\frac{(r_{low}^+ + x_{low}^+)}{(r_{low}^- + x_{low}^-)} \\ &+ \sum_{i=1}^{n}\frac{\sigma_1^i}{L}\frac{1}{4\pi}\left(r_{up}^+ + r_{low}^+ - r_{up}^- - r_{low}^-\right) + q_0 z\end{aligned} \qquad A\,(13)$$

$$\begin{aligned}q_x = &\sum_{i=1}^{n}\frac{\sigma_1^i}{4\pi L}\ln\frac{(r_{up}^+ + x_{up}^+)(r_{low}^- + x_{low}^-)}{(r_{up}^- + x_{up}^-)(r_{low}^+ + x_{low}^+)} \\ &- \sum_{i=1}^{n}\frac{\sigma_0^i + \frac{\sigma_1^i}{L}\left[x + \frac{D}{2} + L(2i-1)\right]}{4\pi}\left(\frac{1}{r_{up}^+} - \frac{1}{r_{up}^-}\right) \\ &+ \sum_{i=1}^{n}\frac{\sigma_0^i + \frac{\sigma_1^i}{L}\left[x - \frac{D}{2} + L(2i-1)\right]}{4\pi}\left(\frac{1}{r_{low}^+} - \frac{1}{r_{low}^-}\right) \\ &- \sum_{i=1}^{n}\frac{\sigma_1^i}{4\pi L}\left(\frac{x_{up}^+}{r_{up}^+} + \frac{x_{low}^+}{r_{low}^+} - \frac{x_{up}^-}{r_{up}^-} - \frac{x_{low}^-}{r_{low}^-}\right)\end{aligned} \qquad A(14)$$

$$q_y = -\sum_{i=1}^{n}\frac{\sigma_0^i + \frac{\sigma_1^i}{L}\left[x + \frac{D}{2} + L(2i-1)\right]}{4\pi}\left(\frac{y}{r_{up}^+(r_{up}^+ + x_{up}^+)} - \frac{y}{r_{up}^-(r_{up}^- + x_{up}^-)}\right)$$

$$+\sum_{i=1}^{n}\frac{\sigma_0^i+\frac{\sigma_1^i}{L}\left[x-\frac{D}{2}+L(2i-1)\right]}{4\pi}\left(\frac{y}{r_{low}^{+}\left(r_{low}^{+}+x_{low}^{+}\right)}-\frac{y}{r_{low}^{-}\left(r_{low}^{-}+x_{low}^{-}\right)}\right)$$

$$-\sum_{i=1}^{n}\frac{\sigma_1^i}{4\pi L}\left(\frac{y}{r_{up}^{+}}+\frac{y}{r_{low}^{+}}-\frac{y}{r_{up}^{-}}-\frac{y}{r_{low}^{-}}\right) \qquad A(15)$$

$$q_z=-\sum_{i=1}^{n}\frac{\sigma_0^i+\frac{\sigma_1^i}{L}\left[x+\frac{D}{2}+L(2i-1)\right]}{4\pi}\left(\frac{z}{r_{up}^{+}\left(r_{up}^{+}+x_{up}^{+}\right)}-\frac{z}{r_{up}^{-}\left(r_{up}^{-}+x_{up}^{-}\right)}\right)$$

$$+\sum_{i=1}^{n}\frac{\sigma_0^i+\frac{\sigma_1^i}{L}\left[x-\frac{D}{2}+L(2i-1)\right]}{4\pi}\left(\frac{z}{r_{low}^{+}\left(r_{low}^{+}+x_{low}^{+}\right)}-\frac{z}{r_{low}^{-}\left(r_{low}^{-}+x_{low}^{-}\right)}\right)$$

$$-\sum_{i=1}^{n}\frac{\sigma_1^i}{4\pi L}\left(\frac{z}{r_{up}^{+}}+\frac{z}{r_{low}^{+}}-\frac{z}{r_{up}^{-}}-\frac{z}{r_{low}^{-}}\right) \qquad A(16)$$

with

$$r_{up}^{+}=\sqrt{\left(x+(2i-1)L+\frac{D}{2}\right)^2+y^2+z^2},\qquad x_{up}^{+}=x+(2i-1)L+\frac{D}{2} \qquad A(17)$$

$$r_{up}^{-}=\sqrt{\left(x+(i-1)2L+\frac{D}{2}\right)^2+y^2+z^2},\qquad x_{up}^{-}=x+(i-1)2L+\frac{D}{2} \qquad A(18)$$

$$r_{low}^{+}=\sqrt{\left(x+(2i-1)L-\frac{D}{2}\right)^2+y^2+z^2},\qquad x_{low}^{+}=x+(2i-1)L-\frac{D}{2} \qquad A(19)$$

$$r_{low}^{-}=\sqrt{\left(x+(i-1)2L-\frac{D}{2}\right)^2+y^2+z^2},\qquad x_{low}^{-}=x+(i-1)2L-\frac{D}{2} \qquad A(20)$$

where q_0 is the groundwater flow rate [L/T], D is the central packer length [L], σ_0^i, σ_1^i are the strength coefficients of ith segment [L^2/T], and L is the half length of line segment [L].

Appendix B

SC#	D(m)	2Δ (m)	Q(m^3/d)	A(m^2)	SC#	D(m)	2Δ (m)	Q(m^3/d)	A(m^2)
1	0.1	0.1	2	1.30	27	0.5	0.3	4	4.59
2	0.2	0.1	2	1.63	28	0.1	0.5	4	3.90
3	0.3	0.1	2	1.91	29	0.3	0.5	4	4.59
4	0.4	0.1	2	2.26	30	0.5	0.5	4	5.21
5	0.5	0.1	2	2.52	31	0.1	0.1	6	2.58
6	0.1	0.2	2	1.65	32	0.3	0.1	6	3.90
7	0.3	0.2	2	2.29	33	0.5	0.1	6	4.90
8	0.5	0.2	2	2.81	34	0.1	0.3	6	3.87
9	0.1	0.3	2	1.90	35	0.3	0.3	6	4.92
10	0.2	0.3	2	2.26	36	0.5	0.3	6	5.82
11	0.3	0.3	2	2.49	37	0.1	0.5	6	4.94
12	0.4	0.3	2	2.81	38	0.3	0.5	6	5.78
13	0.5	0.3	2	2.97	39	0.5	0.5	6	6.61
14	0.1	0.4	2	2.32	40	0.1	0.1	8	3.01
15	0.3	0.4	2	2.67	41	0.3	0.1	8	4.65
16	0.5	0.4	2	3.16	42	0.5	0.1	8	5.81
17	0.1	0.5	2	2.43	43	0.1	0.3	8	4.63
18	0.2	0.5	2	2.77	44	0.3	0.3	8	5.79
19	0.3	0.5	2	2.98	45	0.5	0.3	8	6.81
20	0.4	0.5	2	3.20	46	0.1	0.5	8	5.80
21	0.5	0.5	2	3.40	47	0.3	0.5	8	6.83
22	0.1	0.1	4	2.02	48	0.5	0.5	8	7.70
23	0.3	0.1	4	3.09	SW_1	N/A	1.5	2	3.28
24	0.5	0.1	4	3.90	SW_2	N/A	1.5	4	6.93
25	0.1	0.3	4	3.08	SW_3	N/A	1.5	6	8.99
26	0.3	0.3	4	3.90	SW_4	N/A	1.5	8	12.15

SC# - Simulation case number

Note that the injection cost or injection volume Qt_p is not listed in the above table. When the large Qt_p is applied by using either a high injection rate Q (e.g., >2 m^3/d) or large pulsed injection time t_p (e.g., >0.2 days), the downstream coverage area of dipole is smaller than that of single well.